Title

Can an Off-Nominal Landing by an MMRTG-Powered Spacecraft Induce a Special Region on Mars When No Ice Is Present?

Journal

Astrobiology, 19(11)

ISSN

1531-1074

Authors

Shotwell, Robert F

Hays, Lindsay E

Beaty, David W

et al.

Publication Date

2019-11-01

DOI

10.1089/ast.2017.1688

Peer reviewed

Can an Off-Nominal Landing by an MMRTG-Powered Spacecraft Induce a Special Region on Mars When No Ice Is Present?

Robert F. Shotwell,[1] Lindsay E. Hays,[1] David W. Beaty,[1] Yulia Goreva,[1] Thomas L. Kieft,[2] Michael T. Mellon,[3] George Moridis,[4] Lee D. Peterson,[1] and Nicolas Spycher[4]

[1] Jet Propulsion Laboratory/California Institute of Technology, Pasadena, California. [2] Biology Department, New Mexico Tech, Socorro, New Mexico. [3] The Johns Hopkins University Applied Physics Laboratory, Laurel, Maryland. [4] Lawrence Berkeley National Laboratory, Berkeley, California.

Abstract

This work aims at addressing whether a catastrophic failure of an entry, descent, and landing event of a Multimission Radioisotope Thermoelectric Generator-based lander could embed the heat sources into the martian subsurface and create a local environment that (1) would temporarily satisfy the conditions for a martian Special Region and (2) could establish a transport mechanism through which introduced terrestrial organisms could be mobilized to naturally occurring Special Regions elsewhere on Mars. Two models were run, a primary model by researchers at the Lawrence Berkeley National Laboratory and a secondary model by researchers at the Jet Propulsion Laboratory, both of which were based on selected starting conditions for various surface composition cases that establish the worst-case scenario, including geological data collected by the Mars Science Laboratory at Gale Crater. The summary outputs of both modeling efforts showed similar results: that the introduction of the modeled heat source could temporarily create the conditions established for a Special Region, but that there would be no transport mechanism by which an introduced terrestrial microbe, even if it was active during the temporarily induced Special Region conditions, could be transported to a naturally occurring Special Region of Mars.

1. Executive Summary

NASA recently requested an update to the analysis previously done for the Mars Science Laboratory (MSL) mission (summarized in Hecht and Vasavada, 2006) to examine the hypothetical off-nominal scenarios wherein a radioisotope-powered lander has a moderate velocity impact on the martian surface. The question of interest was “would such scenarios create a temporary spacecraft-induced Special Region?” In the MSL analysis, the starting assumption was that water ice might have existed at some percentage mixed into the volume of the material affected. In the present analysis, which has been broadened to encompass the conditions relevant to the Mars 2020 mission, no water ice is assumed present; however, we now consider the case in which hydrated minerals—when heated sufficiently—can release their bound water, generating similar potential for an induced Special Region. This case arose as a result of the MSL *in situ* findings (as well as

supporting evidence from other Mars spacecraft), confirming both the lack of existing water ice in the near subsurface at the landing locations and the detection on Mars of several minerals that contain water in a bound state (*e.g.*, allophane, opal, potentially Ca-perchlorate).

The validation of our primary model was performed by researchers from the Lawrence Berkeley National Laboratory (LBNL) who had also participated in the parallel MSL analysis (Hecht and Vasavada, 2006) and who routinely perform multiphase, geochemical modeling for terrestrial applications. The mission failure scenarios were revisited, as were the starting conditions for various surface composition cases to establish the worst-case scenario. In parallel, an independent effort was started at the Jet Propulsion Laboratory to produce a comparable modeling environment with a different modeling tool set to evaluate assumption-dependent modeling outcomes, to execute alternative scenarios, and also to perform a limited set of sensitivity analyses. This model will be referred to as the secondary model.

The summary outputs of both modeling efforts showed similar results, thus providing confidence that the models accurately reflect features of the scenarios. Not surprisingly, it was found that a thermal source such as a fully intact general purpose heat source (GPHS) module if it were embedded at a maximum depth into the subsurface, due to a moderate-speed impact, could heat local minerals to sufficient temperatures to release water from the minerals' crystal structure. We did not attempt to distinguish whether the mineralogic dehydration reactions initially released their water as liquid or vapor—this was not deemed important for the questions at hand (although by paying attention to the temperature of these dehydration reactions, this could be determined). The released water would migrate away from the heat source in the vapor phase and condense as water or freeze as ice as it moved to the cooler surrounding ground. Water would continue to be released, and eventually a small boundary layer of liquid water would develop inside the ice layer across the thermal gradient induced by the heat source. In some locations and for limited time, the thresholds of temperature and water activity (a_w) currently used to define a planetary protection Special Region could be exceeded.

These Special Region conditions would be temporary, however, and very soon only thin water film conditions would exist, thereby preventing any microbial transport into or out of the liquid zone. The total extent of the water–ice shell that would form is predicted to extend up to several meters from the heat source. The conditions for liquid water to exist at the surface are not observed in the models. As the system progresses, the models show that heat and water vapor would be lost to the atmosphere, such that thermal equilibrium would be reached in about 1 year. Because water vapor would be progressively lost to the atmosphere over time through evaporation and sublimation, eventually both the water and water–ice shells would disappear. During the time when the Special Regions thresholds could be exceeded in the subsurface, there is no viable transport mechanism from

that volume of regolith or rock to naturally occurring Special Regions in the environment. Eventually, the heat source would desiccate the volume of material, and any terrestrial microbes there would starve to death. Thus, we conclude that this type of impact would not constitute “harmful” contamination (Outer Space Treaty, 1967).

2. Introduction

2.1. What is the problem to be solved?

NASA has announced plans to send a rover to Mars in the 2020 launch opportunity. This rover is similar in many respects to the Curiosity rover (MSL) (Bernard and Farley, 2016) and is similarly being designed to be powered by a radioisotope system (Hammel *et al.*, 2013). As part of the planning for the launch of MSL (in 2011), it was recognized that in certain potential failure scenarios related to the landing sequence (*e.g.*, if the parachute failed to open) the impact on the martian surface could inject spacecraft debris, including Multimission Radioisotope Thermoelectric Generator (MMRTG) heat source into the subsurface. The same concerns would apply to the Mars 2020 mission, as well as any other future Mars mission that makes use of such a power system.

In the early phases of MSL's landing site selection process (summarized by Grant *et al.*, 2010 and Golombek *et al.*, 2012), sites as far north as 60° latitude were considered. However, the neutron and gamma ray spectrometer investigations on the 2001 Mars Odyssey mission (ODY) discovered significant quantities of ice on Mars within 1 m of the surface at that latitude (Boynton *et al.*, 2002; Feldman *et al.*, 2002; Mitrofanov *et al.*, 2002), and geological arguments of recent glacial features (*e.g.*, Dickson *et al.*, 2012) supported the possibility that ice could be present in the martian subsurface within a depth of 5 m at latitudes as low as about 30°, both north and south latitude. Since these potential landing sites could have had shallow subsurface ice, this raised questions about whether the MMRTG could melt the ice and create what is referred to as an “induced Special Region” (Beaty *et al.*, 2006; Rummel *et al.*, 2014). This led to a detailed analysis led by Brian Muirhead of the planetary protection implications of such scenarios (summarized by Hecht and Vasavada, 2006). Ultimately, potentially ice-containing landing sites were dropped from consideration for MSL, and the final landing site choice (Gale Crater) is at a latitude of 4.5°S and is ice-free.

For the Mars 2020 mission, none of the candidate landing sites shows evidence of ice within 5 m of the surface (see Fig. 45 of Rummel *et al.*, 2014), although the evidence is still to be weighed. At such ice-free sites, it would obviously not be possible to create an induced Special Region by the melting of ice. However, recent discoveries by the 2003 Mars Express Mission, the 2005 Mars Reconnaissance Orbiter (MRO), the 2007 Mars Phoenix mission, and by MSL have raised a different concern: Hydrated minerals exist in the martian rocks and regolith (Ehlmann and Edwards, 2014). Could the impact

of an MMRTG into rock/regolith create an induced Special Region by causing the MMRTG to heat a volume of material above the dehydration temperature of the water-bearing minerals, and having done so could the resulting liquid or condensed water vapor be concentrated in a way that would exceed the a_w threshold for Special Regions?

The potential damage to Mars ("harmful contamination," in the phrasing of the 1967 Outer Space Treaty) would come not just from local, short-term consequences at an impact site but also from the possibility that Earth-sourced microbes could disperse from that site to a naturally occurring Special Region in some nearby environment, and proliferate there. Thus, in this analysis we have evaluated not just the evolving thermodynamic conditions at the impact site but also the possibility of transport pathways to other parts of Mars.

Note that based on thermodynamic arguments (Rummel *et al.*, 2014), the process of natural mineral deliquescence (the ability of a mineral to release brine when the temperature is raised) by itself cannot produce simultaneous temperatures and water activities that would qualify as a Special Region. As such, natural mineral deliquescence is not considered further in this study.

2.1.1. Problem statement

In the event of a catastrophic failure of an MMRTG-based lander entry, descent, and landing (EDL) event, could embedding MMRTG into the martian subsurface: (1) create a local environment that would temporarily satisfy the conditions for a martian Special Region that is conducive to terrestrial organism reproduction and (2) establish a transport mechanism through which introduced terrestrial organisms could be mobilized to naturally occurring Special Regions elsewhere on Mars (surface or subsurface)?

2.2. Methodology

Our approach has three primary components.

(1) The first component is a basic physical scenario (reported in Section 3), with primary initial and boundary conditions. Our ability to run multiple models was limited by time and money, so we focused on a single basic physical scenario. Where choices in assumptions were necessary, we attempted to choose plausible conditions that would be most favorable to biological potential (*i.e.*, "worst case"), and we then evaluated sensitivities about that.

(2) Next, we provide a definition of the geological assumptions/inputs to the numerical models that relate to the volume of rock/regolith evaluated (reported in Section 4). We

used a mixture of plausible values and worst-case values. Simply assigning all parameters to their worst-case values for this aspect would have resulted in the definition of a pathological case for which the general usefulness would have been questionable.

(3) The final component is numerical modeling (reported in Section 5) that was used to develop quantitative estimates of time, temperature, spatial parameters, fluid behavior, and mass flux. We ran one primary model and a follow-up secondary model; both are described next.

(4) We next present a general analysis of the expected evolution of the system with time (Section 6), followed by the results of the numerical modeling (Section 7).

(5) Finally, we discuss and interpret the biological potential based on the physical results (Section 8).

3. The Basic Physical Scenario

The initial assumption for this modeling began with the hypothetical scenario of a catastrophic failure of a skycrane-based EDL System, such as on the Mars 2020 rover mission, that would cause a moderate velocity impact (approximately 300–500 m/s) on the surface. These impact parameters (and other engineering details) are the same as in the scenario modeled by a large team (of which several of the authors of this report were members) led by Brian Muirhead in ~2004 (Hecht and Vasavada, 2006) for the MSL mission, although in that case the target was assumed to be ice-rich. We assume that the impact would discharge the intact GPHS modules from the MMRTG into the shallow subsurface. We assume that the overall MMRTG consists of nine GPHS modules (250 thermal W each), each of which is composed of four fuel pellets (62.5 thermal W each) derived from 150 g of PuO_2 per fuel pellet. The dimensions of each GPHS module are $6.25 \times 6.25 \times 10$ cm, with a mass of 1.6 kg.

In constructing the impact scenario to be modeled, there are multiple choices to be made, and in each case we have selected the worst-case option. First, of the multiple possible failure modes during the EDL sequence, the one that is modeled here is failure of the parachute to deploy. This would result in the breakup of the rover as a whole, with major pieces remaining intact during descent, including the MMRTG. Other scenarios (Fig. 1) would

include pre-entry failure or failure during entry, which would result in the tumbling of the entry vehicle and the release of major elements, such as the rover, which would individually impact the regolith at a very high velocity. This extremely high-velocity impact would create a large crater, but it would also break the rover into pieces with almost no emplacement into the regolith. A failure later in the sequence, such as during the powered descent phase, would involve a crash into the surface of the rover as a whole, but at a much lower velocity that would also not result in emplacement of the heat source into the regolith.

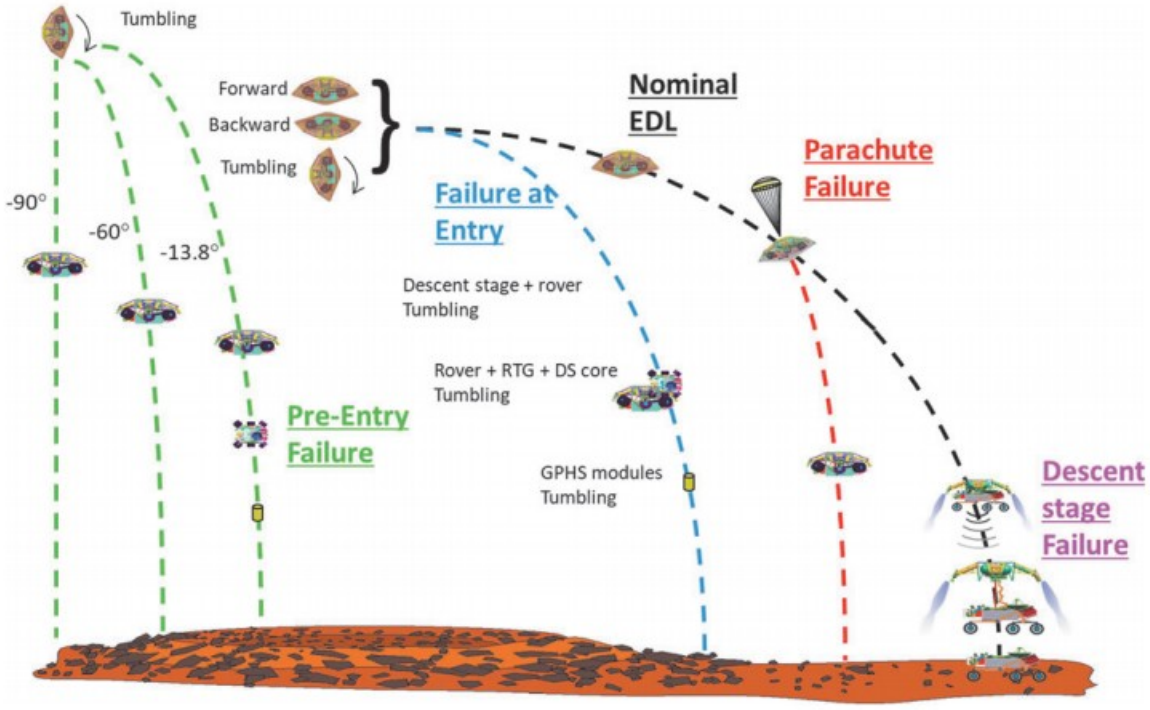

FIG. 1. Potential failure scenarios and breakup sequences during EDL at Mars. Note that the case modeled in detail is that of the parachute failure, shown in red, which is considered the most threatening from a biological perspective. EDL, entry, descent, and landing.

In the intermediate case (Fig. 1), where loss of control occurs supersonically, pieces of the heat source would impact the surface at 300–500 m/s. Thus, lower velocities would maintain the entire MMRTG thermal source whole, but without any penetration depth, and higher velocities would further break apart the GPHS modules, and would result in scattering of the individual 62.5-W pellets. The GPHS modules, however, are sufficiently large and cohesive that they would penetrate to depth and deliver significant heat into the subsurface. It was estimated that in low-strength regoliths, the GPHS module could remain cohesive at impact speeds up to ~450 m/s. The maximum depth of penetration would be achieved when the module is oriented along its narrow face, and this was chosen for this analysis.

Another consideration was the structure of the subsurface: regolith, bedrock, or some combination (Fig. 2). The compressive strength of bedrock is such

that the GPHS would break apart if it hit it, and maximum heating would happen if the radioactive material stays concentrated, rather than dispersed. Therefore, the maximum depth of penetration for an impact of the assumed velocity would happen in regolith (which has low density and low compressive strength). Previously unpublished calculations show that a penetration depth of 0.89 m would be achieved through a regolith-only subsurface environment. Since the thermal conductivity of regolith is lower than rock (*i.e.*, it acts as an insulator), the heat would be more concentrated, and there would be a greater increase in the local temperature. However, we have no *a priori* way of knowing whether this is a worst case or not. The quantity of water released by dehydration reactions depends on both the volume heated and the magnitude of the temperature increase.

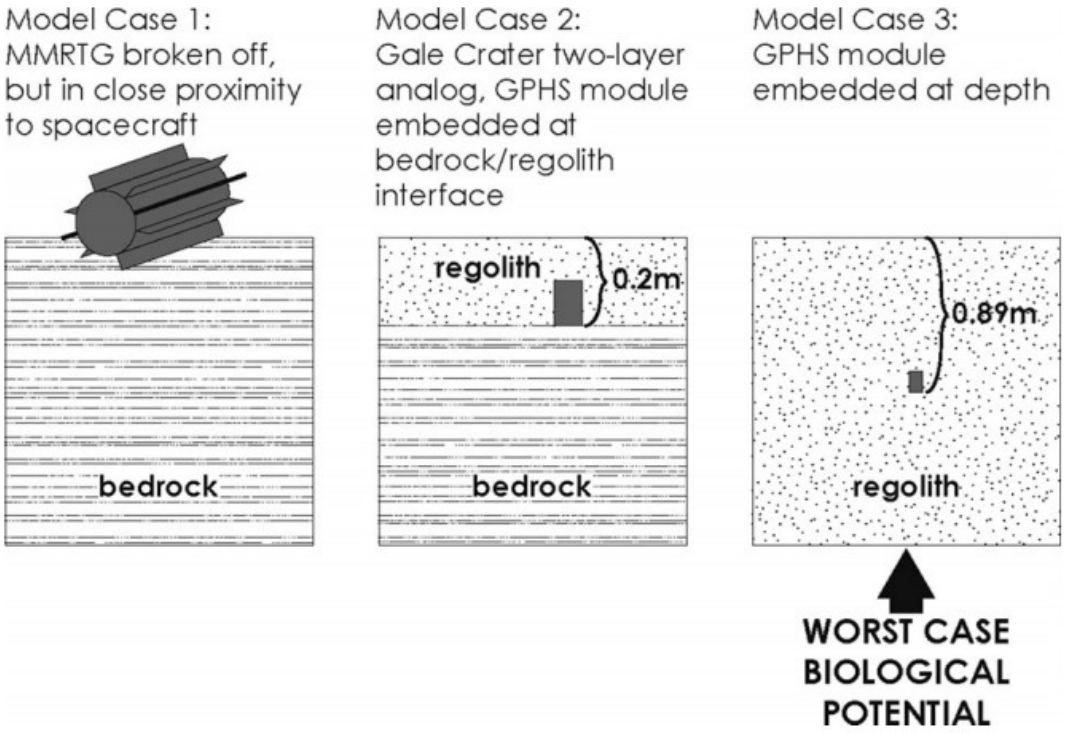

FIG. 2. Schematic cross-sections showing the three possible subsurface cases considered. Case 1 is an impact into bedrock, Case 2 is an impact into 0.2 m of regolith overlying bedrock (using the depth of the two-layer subsurface derived from DAN analysis) (Litvak *et al.*, 2014), and Case 3 is an impact into regolith where the depth to bedrock is deeper than the limits of the scenario. In all cases, the bedrock compressive strength was modeled as 20–80 MPa, and the regolith as 0.5 KPa. The bedrock was assumed to have 10% water equivalent in Case 1 and 4.1% water equivalent in Case 2; and the regolith was assumed to have 1% water equivalent in Case 2 and 6.6% water equivalent in Case 3. Case 3 was judged to be of the greatest concern from the point of view of biological potential (as described in Section 3), so this is the case that was modeled in detail. DAN, Dynamic Albedo of Neutrons.

Three further assumptions were made to set up the physical model. First, due to the low compressive strength and high porosity of the regolith, we assume that the penetration column that the GPHS module entered would fill in completely behind the module, leading to a heat source that was covered completely by regolith (Fig. 3). Having the GPHS covered is a worse case than having it exposed; having an open column would provide a heat leak

and increased energy exchange to the atmosphere, as well as removing material from the affected zone to release water. Second, during this emplacement, we assume that some viable terrestrial organisms are discharged into the column region along with the heat source, or scattered into the regolith nearby. We further assume that organisms could not be implanted to a lower depth than the heat source, as the GPHS modules have the highest ballistic coefficient (Fig. 3). In essence, we assume a scattering of terrestrial organisms very near the thermal source impact location and that these microbes remain viable at the start of the analysis. This is clearly a worse case than having no organisms at these positions. Third, to construct a worst case for water–ice longevity, winter thermal starting conditions were assumed, with both atmospheric and subsurface temperatures at 183 K (−90°C). Higher assumed initial temperatures would result in higher subsurface temperatures and would more rapidly evaporate a water–ice shell in the vicinity of the surface.

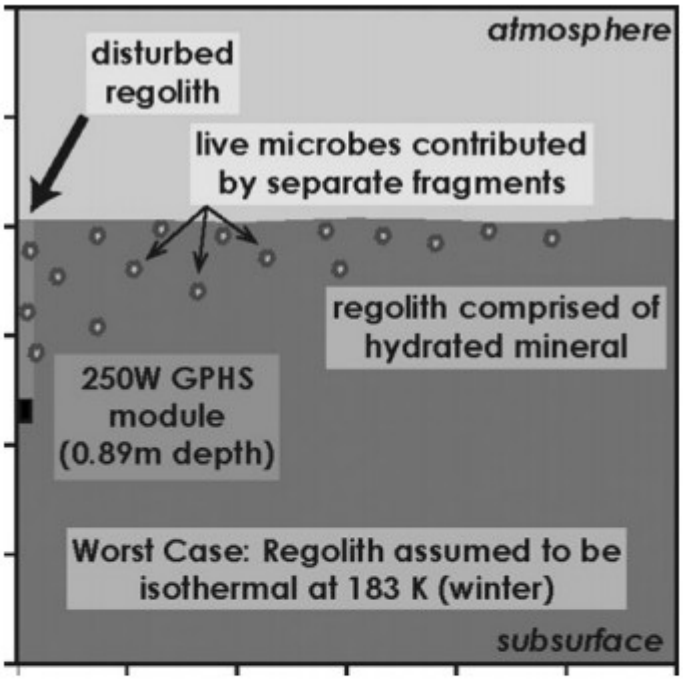

FIG. 3. Schematic cross-section showing assumed starting conditions for the numerical modeling. A moderate velocity (approximately 300–450 m/s) impact would discharge the GPHS modules and allow them to penetrate 0.89 m into the regolith. The penetration column is assumed to be backfilled by regolith. Terrestrial microbes (small stars) might be discharged into the column region, or/and scattered into the regolith nearby along with other spacecraft debris. The microbes and other spacecraft debris would have a lower ballistic coefficient than the GPHS module, so they would have a lower penetration depth. No organisms would be present below the heat source. GPHS, general purpose heat source.

4. Geological Inputs into the Models

Although orbital data can provide some indication of surface mineralogy, there is no way of determining all of the geological aspects of the regolith at the next landing site from orbital data alone. We decided to use the best data that have been collected directly from the surface on regolith mineralogy, porosity/permeability, and grain size distribution, and we established the models by using MSL data from Gale Crater, letting that be a proxy for Mars. This is not to say that the next landing site will be identical to Gale Crater in these respects, but it is more realistic than constructing a pathological worst-case regolith that may not exist anywhere on Mars, and more information exists for this location than any other on Mars. Sensitivity to various parameters was performed to understand the degree to which uncertainty in any of the physical parameters would influence the results. The worst-case conditions were selected for many aspects of the scenarios

with the goal of identifying the worst possible contamination scenario to test how easily terrestrial microbes could be spread. Table 1 summarizes the starting conditions; further details are in Appendix 1.

Table 1. Mineralogy and Geological Details Used as Inputs to The Model

Material	*Distribution*	*Quantity (wt %)*	*Grain density (g/cc)*	*H_2O (wt %)*	*Temp H_2O released (°C)*
Opal	Amorphous component (veins, randomly distributed)	36.4	2.10	15.0	>400
Plagioclase	Homogeneous mixture	24.1	2.70	—	—
Fe-forsterite	Homogeneous mixture	13.3	3.80	—	—
Augite	Homogeneous mixture	8.7	3.40	—	—
Pigeonite	Homogeneous mixture	8.2	3.40	—	—
Allophane	Amorphous component (veins, randomly distributed)	3.0	1.90	20.0	90
Ca-perchlorate	Amorphous component (veins, randomly distributed)	1.5	2.50	37.6	~80
Magnetite	Homogeneous mixture	1.2	5.10	—	—
Anhydrite	Homogeneous mixture	0.9	2.97	—	—
Quartz	Homogeneous mixture	0.8	2.65	—	—
Sanidine	Homogeneous mixture	0.7	2.52	—	—
Hematite	Homogeneous mixture	0.6	5.15	—	—
Ilmenite	Homogeneous mixture	0.6	4.72	—	—
	Total			6.6	

The three amorphous components add up to 40.9 wt %. With assumed 37% porosity for the regolith and the weighted average grain density, the overall density for the regolith is ~1.7 g/cc.

Note that by comparison to similar problems on Earth for which this numerical model has been run, dry martian regolith has a very low thermal conductivity (Presley and Christensen, 1997). The volume affected by heating would be relatively small, and the amount of heating within that volume would be relatively high. The martian regolith has insulating properties (on the order of that of Styrofoam) that are outside our normal experience here for soils on Earth. See Appendix 1 for more details.

5. The Numerical Simulation

5.1. Model 1: (primary model, LBNL): TOUGH + Real Gas Brine

The described scenario was modeled by using a modified version of the TOUGH+RealGasBrine (hereafter referred to as T+RGB) code (Moridis and Freeman, 2014a, 2014b). For the purpose of this article, we refer to this model as the “primary model.” Modeling details are contained in a companion paper (Simulation of Coupled Flow, Thermal and Geochemical Processes in Response to a Heat Source Buried in the Martian Subsurface are detailed by Moridis and Pruess, 2006). T+RGB describes the nonisothermal flow of an aqueous phase and a gas mixture in a gas-bearing medium, and it is based on the Integral Finite Difference method (Narasimhan and Witherspoon, 1976), a member of the Finite Volume family of methods (Edwards, 1972). Up to 12 individual gases can be tracked, and salt can precipitate as solid halite. The T+RGB code allows the study of flow and transport of fluids and heat over a wide range of time frames and spatial scales in gas reservoirs and in any problem involving the flow of gases in geological media. For this study, this code was applied to simulate coupled

flow and thermal effects, including nonideal behavior of gas mixtures, Darcy flow, and equilibrium gas solubility into water. Geomechanical, gas sorption, and non-Darcy flow effects, which can also be simulated with T+RGB, were not considered here because they are unlikely to occur under the conditions of this problem. Because of its fully implicit formulation that involves the Newton-Raphson iteration and solution of the resulting Jacobian (using several options of preconditioned conjugate gradient solvers), T+RGB is unconditionally stable and can seamlessly handle the phase changes, state transitions, strong nonlinearities, and steep solution surfaces that are expected in the martian problem at hand.

The water properties module in T+RGB was extended into the ice range to cover the entire phase diagram of water. Thus, in the modified code, the water properties are accurately described over a Mars-relevant temperature range (505–2272 K) and a pressure range from 0 to 1000 MPa by using the most recent data and relationships (International Association for the Properties of Water and Steam [IAPWS], 2009, 2011; Wagner and Pruss, 2002). The number of possible mass components in the extended code was increased from two (H_2O+CO_2) or three (H_2O+CO_2+Salt) to six by the addition of the three hydrated minerals assumed to be part of the target composition (perchlorate, allophane, and opal. These are known or suspected Mars hydrated components in the MSL Rocknest sample for which satisfactory thermodynamic data could be found in the literature. Note that other hydrated minerals have been identified in other places on Mars, including gypsum, kieserite, epsomite, and smectite, but they were not modeled in this study. In addition, the possible number of phases was increased from two (aqueous+gas) or three (aqueous+gas+halite) to five (aqueous+gas+halite+ice+a solid phase that comprises the 3 hydrated martian minerals), into which the six components were distributed.

Note that the code did not include a liquid or solid phase for carbon dioxide because preliminary scoping calculations showed that such phases were precluded under the martian conditions considered in this study ($P = 845$ Pa and $T = 183$ K/−90°C). In the absence of kinetic information on the subject, the dehydration reactions of the three minerals were treated as following an equilibrium model. This approach resulted in a worst-case scenario, as it corresponded to the fastest possible release of H_2O once the enthalpy needs of the dehydration equation were satisfied. Finally, the thermal properties module of T+RGB (describing the thermal conductivity and the specific heat of the various media) was extended to describe the specific properties of the regolith as functions of temperature and water content following the approach of Piqueux and Christensen (2009b).

The model involved fluid (aqueous and gas) flows through the domain, and it was constructed to place quantitative constraints on the rates, distance scales, temperature, a_w, and possibilities for fluid flow within the thermal anomaly. The focus of this model was on the parameters that were relevant to interpreting the possibility of generating an induced Special Region, and of

the possibility of communication between this anomalous region and naturally occurring Special Regions elsewhere on the planet.

For these simulations, carbon dioxide was assumed to be the only noncondensable gas. The study monitored the flow and accumulation of water in its various states, carbon dioxide, and the three minerals discussed earlier solving six simultaneous equations (five describing the mass balance of the mass components, and the sixth describing the heat balance of the entire system). The cubic equations of state describing the properties of the gas phase are from Moridis *et al.* (2008; WebGasEOS; Reagan, 2008). Gas dissolution into the aqueous phase is from the equation of fugacities, accounting for a_w and the effect of salts. The system conductivity was varied as a cylindrical axisymmetric domain, as a function of temperature and water saturation* level. The spatial domain of 171 cm (radius) × 273 cm (depth) was discretized into ~40,000 elements. The element size was determined from scoping calculations: It was nonuniform, with very fine vertical and radial discretizations (ranging from 0.5 to 1 cm) in the all-important vicinity of the heat source, that is, within 1 m from the source; beyond this distance, the vertical and radial discretizations followed a logarithmic distribution to the end of the domain. The temporal discretization in this fully implicit model was controlled by the convergence criterion (the mass and heat balance error tolerance of 0.001%), not by the user, and resulted in time steps ranging from 2 to 1.4×10^4 s. The 3.73-m/s^2 martian gravity was included in the model. The full model was run to 200 sols of Mars time for a case with no Ca-perchlorate, and to 300 sols when Ca-perchlorate was considered. The overall lifetime of the thermal anomaly is considerably longer than this (note, *e.g.*, that the half-life of the plutonium heat source is 88 years), but as discussed in Section *6.2. Water behavior overview*, it is during the early stages of this scenario that most of the liquid water would be present, and when conditions would be changing most rapidly.

5.2. Model 2: (secondary model, JPL): Sierra-Aria

The objectives of a second model, which for the purpose of this article we refer to as the “secondary model,” were to assess the sensitivity of the primary LBNL simulation results to boundary conditions (thermal and gravity), to assess the effects of mesh size and extent, and to provide an independent confirmation of the primary model results by using simplified geochemical models of the mineralogic water release.

This simulation was developed in the Sierra “Aria” Thermal-Fluid multiphysics platform. Sierra is a mechanical analysis suite developed at Sandia National Laboratories (SIERRA Thermal/Fluid Development Team, 2016). The model was constructed as a two-dimensional axisymmetric mesh, with the GPHS positioned on the axis. The baseline mesh domain was 5 m in radius and 5 m in depth, and included >100,000 nodes, with significant refinement near the GPHS out to a distance of ~1 m. The size and density of the mesh were varied as part of the sensitivity study and were found to be

important considerations for predicting the long-term evolution of the water shell.

Thermal boundary conditions were applied to the three surfaces of the domain, and they were varied as well. Both an isothermal and a diurnal variation condition were alternately applied to the top surface. The regolith was modeled as a porous medium with conductivity that depended on the saturation of the liquid phase, using the model shown in Fig. A1 of Edwards and Piqueux (2016). The original conductivity of the regolith would be very low in the dry state, but it would rise rapidly as water is released. The model included the effects of regolith melting, which changes both the heat capacity and the thermal conductivity.

Sierra-Aria includes preconfigured multiphase transport models for several common component combinations found in terrestrial applications. It also includes a generalized multiphase chemistry and transport capability that might be tailored to our martian conditions. For expediency, however, we chose an approximate single-phase transport model with multiphase effects incorporated into the fluid physical properties. For example, solidification was modeled by using a temperature-dependent viscosity within the porous transport model.

The water properties as a function of temperature and pressure were determined from a standard water-phase diagram, ignoring thin film transport and salinity effects. The water vapor pressure at a given temperature was used to divide the properties into either a gas or condensed state. The ideal gas law was used for the gas state below the vapor pressure. Above the vapor pressure, the condensed state was modeled as a transitional “slush” region from solid (ice) conditions below the triple point, to liquid conditions above. The minimum width of the slush zone was found to be 20°C due to numerical conditioning. This use of a slush zone in the model lowers the melting temperature in a similar way to an increase in salinity by at least 10 wt %. The viscosity was also varied to simulate the liquid–solid transition, with the solid modeled as a fluid with 10,000 times the viscosity of the liquid phase. The water release from the regolith was modeled by using a first-order Arrhenius reaction model.

The simulation time steps used the internal Sierra adaptive time stepping mechanism to control numerical accuracy. This proved to be an important consideration in ensuring numerical stability in the simulation. Initially, as the regolith begins to heat and water would be initially released, the solution transients are relatively sharp, requiring very small time steps. However, the simulation eventually achieves a quasi-steady state condition for which larger time steps were possible, similar to the primary model.

6. The Flow of Heat and Water in Response to a GPHS Module: General Considerations

6.1. Heat flow overview

The main objective in the modeling was to assess whether the heat flow from the GPHS module would increase temperatures within the local environment enough to cause the decomposition of hydrated minerals, and to cause the released water to accumulate in a liquid state, as required for biological activity. Initially, the heat added to the system would cause the temperature to increase locally (Fig. 4). The GPHS module and surrounding environments would eventually reach a quasi-stable state when the heat flow into the system (which includes the “module” and a yet-undetermined volume of the surrounding regolith, the size of which would vary as the isotope decays) and the heat flow out of the system are in balance. At that point, temperatures would be relatively stable. As the isotope decays (half-life = 88 years), the heat flux would decline. As heat flux reduces, the temperatures would decrease. Thus, the maximum extent of the affected zone would be realized once the affected zone reaches equilibrium and then would slowly decay with the reduction in thermal output of the heat source.

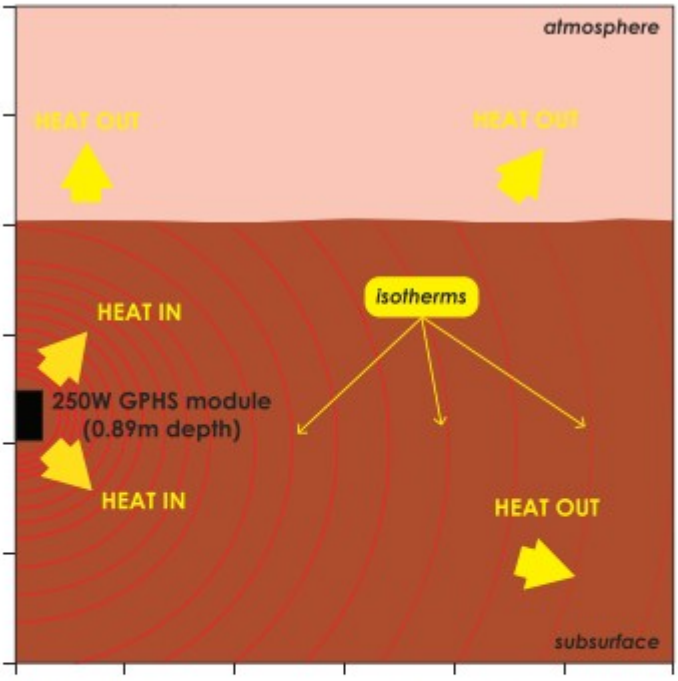

FIG. 4. Schematic cross-section showing the general flow of heat around the embedded 250 W GPHS module. Initially, heat would be added, causing the temperature to increase, and this heat would flow out to the surrounding regolith/rock and to the atmosphere. The GPHS module and surrounding environments would eventually reach a quasi-stable state when the heat in and the heat out are in balance. At that point, temperatures would be relatively stable. As the radioactive isotope in the heat source decays (half-life = 88 years), the heat flow in would decline, and the temperatures would decrease.

6.2. Water behavior overview

6.2.1. Ice and water shells

As specified by assumption, the affected volume would initially contain only ice-free regolith (the absence of ice is a landing site constraint for Mars 2020; see Section 2.1). The very low temperatures in the shallow martian subsurface preclude the existence of liquid water, but a certain amount of H_2O would be present in the hydrated minerals. Since the temperature on Mars increases with depth due to the planetary heat flux, it certainly reaches the melting point of water (273 K) at some depth, but this effect happens at a very different scale than that of the shallow environment we are considering. Assuming a relatively high heat flow of 0.03 W/m^2 (this used to be considered average for Mars but most workers have recently reduced this by $\sim 2\times$), then 273 K would be reached at >110 m (calculated by using $T_{surface} = 183$ K and assuming that the subsurface maintains thermal conductivity at 110 m, *i.e.*, no lithostatic compression). For the purpose of this numerical modeling exercise, therefore, we assume isothermal 183 K initial conditions (Appendix 1).

After the impact, at the core of the thermal anomaly, as the temperature increases, the hydrated minerals would break down when their thermal stabilities are exceeded, and the released water would diffuse outward in the form of water vapor (Fig. 5). This heating would result in a locally dehydrated zone, which would survive until the thermal anomaly dissipates as the radioisotope decays. When the liberated water vapor reaches the boundary of the artificially heated zone and comes into contact with surrounding cooler regions, it would condense in the pore network into a liquid water shell (in the warmer area closest to the heat source) that is enveloped by an outer ice shell (where the temperature is lower). The development of the water and ice shells represents a redistribution of the pre-existing water content; there would be no new water added by the process. As temperatures increase, the ice shell would progressively expand and thicken as the heated zone expands and more water is driven out of the interior. As soon as the process of heat and water vapor loss to the atmosphere begins through sublimation and evaporation at the top of the thermal anomaly, the total amount of water in the local system would begin to decrease (since the atmosphere would behave as an infinite heat and water vapor sink). The heat source would, in effect, be an engine that would progressively pump water out of the system, and the net effect would be one of drying. Individual positions within the volume modeled would thus sequentially experience ice, then water, then hot dry conditions, and finally progressively cooler temperatures as the heat source subsides.

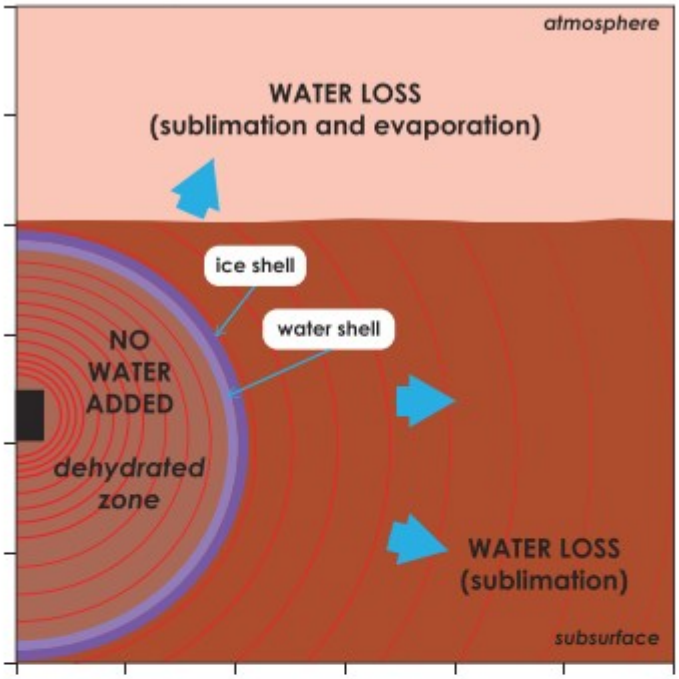

FIG. 5. Schematic cross-section showing the general flow of water around the embedded 250-W GPHS module. The volume of regolith at the time of the RTG burial is assumed to contain hydrated minerals (but neither ice nor liquid water), which would decompose and release water vapor. The water vapor would condense/freeze to water/ice at the appropriate thermal conditions, leaving a dehydrated zone at the core. Under certain conditions, water would be lost to the atmosphere by sublimation from the ice shell, and removed from the system (depicted here); under other conditions, there is a possibility of water vapor moving outward and accumulating as liquid or ice when encountering appropriate regolith temperatures, with minimal losses to the atmosphere. Since no new water would be added, the net effect would be one of drying. The position of the ice shell would progressively expand, and it would then stabilize when the heat losses to the atmosphere stabilize. Contraction of the ice shell is not expected to occur for thousands of years because of the very long half-life of the plutonium source. RTG, Radioisotope Thermoelectric Generator.

Within the water shell, two important things would happen: (1) If perchlorate were present, it would dissolve in the water, affecting parameters such as the water activity, the frost point, and the vapor pressure (*e.g.*, Marion *et al.*, 2010). 2). As the S_{liq} increases, the liquid water would go from existing only as thin films on the mineral grains to being present in the pore network as “free” water. We have not modeled the diameter of the maximum extent of water and ice shells beyond the point where growth is largely asymptotic at ~2.5 m.

6.2.2. Shallow water loss

It would be difficult to maintain shallow water, in either liquid or frozen state, against vapor loss to the atmosphere. In addition, since liquid water is thermodynamically unstable at the martian surface (Section 8.1), its possible occurrence would be limited to the subsurface. First, by using the approach of Mellon *et al.* (2004), it is possible to calculate rates of water loss from a given depth by sublimation and of diffusion through the overlying regolith into the atmosphere in terms of the timescale for a 1-mm recession of the ice table (see their Fig. 5). For the purpose of this calculation, we have used a relatively humid atmosphere with 10 pr μm (precipitatable microns) of water uniformly distributed with CO_2 resulting in a vapor density of 9.6×10^{-10} g/cc, and regolith diffusive properties of 10-μm pores and a tortuosity of 1.5 (Sizemore and Mellon, 2008). In the primary numerical model, at 200 sols, the ice would be at about 5–7 cm depth and have a temperature of about −20°C (253 K). That would imply that the rate of ice loss would be approximately 0.3–0.5 mm of ice per sol. At this high loss rate, latent heat removal will also cool the shallow subsurface by a few K. However, depending on the concentration of ice and liquid, the water above the GPHS module may not last more than a few 10's of sols. Although advection can add to diffusive loss of water (Ulrich, 2009) and is not included in this study, it is mostly negligible in icy regions of Mars, but may increase the loss rate of water by 10% at 250 K, making our results conservative with respect to the time for water and ice shell retention.

In addition, Mellon *et al.* (1997) showed that shallow ice under the influence of an upward flowing thermal gradient will reach and maintain a steady-state depth as it undergoes continued diffusive loss to the atmosphere. By using the analytical model of Mellon *et al.* (1997), adjusting it for the current situation (high heat flow), and assuming dry regolith thermal conductivity of 0.038 W/(m·K) (Appendix 1), it is possible to estimate the depth of the ice in steady-state equilibrium with the atmosphere. The heat flow model indicates that the near-surface gradient would be about 1200 K/m. At equatorial potential landing sites with mean surface temperatures of approximately 215–225 K (Mellon *et al.*, 2004), the steady-state depth would be approximately 8–9 mm below the surface. This depth falls within the diurnal active layer and this is, thus, influenced by cyclic warm mid-day temperatures, creating an “effective steady-state depth” that is slightly deeper at 1–1.5 cm below the surface. During the period leading to steady state, the ice would remain deeper. In fact, the “effective steady-state depth” represents only a limiting case of the most shallow extent of the ice shell. The ice shell cannot get closer to the ground surface than this depth because at shallow depths sublimation loss will always outpace resupply from below. Further, the liquid water would always remain below the ice shell. Also, based on the results of Mellon *et al.* (1997), the net loss of the liquid water shell would precede loss of the ice shell. It seems unlikely that

ice, or especially liquid water, would be able to breach the surface at any time.

Although we have concluded earlier that for the purpose of this article, the top of the ice shell reaches a “steady state,” ice at these shallow depths would be within the diurnal active layer. The concept of steady state is then a matter of scale/context. We have done some scoping calculations to evaluate this—our goal was to constrain an “effective steady state depth” within the diurnal active layer. The graphs of T, liquid, and ice distribution at 200 sols, with and without perchlorate, are most relevant to this question—they show the most shallow ice at roughly 5 cm. The fact that the ice reaches only 5 cm in 200 sols suggests that it is not yet at “steady state.”

We have run additional thermal models to determine the min, mean, and max temperatures and, in particular, the vapor pressures at depth to estimate the loss rates under different conditions. Assuming Jezero Crater soil properties and conditions (but with an albedo of 0.25, Mars average), a mean annual temperature of 217–237 K (compared with the isothermal 183 K assumed in our primary model), a GPHS heat flow of 45 W/m^2, thermal conductivity of 0.038 W/(m·K), and no feedback between ice/liquid content and thermal conductivity, we find that the “effective steady state depth” is pushed a little deeper below the surface, by $<2\times$, due to the effects of the diurnal temperature cycles and the nonlinearity of the vapor density's function of temperature. So instead of 8–9 mm, it would be 10–15 mm (approximately). This does not meaningfully affect the final conclusions of this article.

These calculations also show that the rate of water vapor loss to the atmosphere from within the diurnal active layer at this “effective steady state depth” is enormous. With the high heat flow, the loss rate from 1-cm depth would be about 0.6 $g/(cm^2\cdot sol)$, if 0.6 g of water were even available. This rate is about $10\times$ the rate of water loss estimated from the primary model from a given depth at a fixed mean temperature. The reason for the increase is that within the diurnal active layer, the ice spends some time at warmer temperatures and the vapor pressure is exponentially dependent, skewing the average vapor density relative to the average soil temperature.

At this rate, all the water that accumulates at the top of the ice/liquid shell would be lost in a few sols—faster than it forms. This observation leads us to conclude that the top of the ice/liquid shell nearest the surface would never really form. Although this point seems clear, it is hard to quantify with the existing numerical models.

6.3. Summary of overall sequence from first principles

The overall steps of this sequence are shown in Fig. 6. Our numerical modeling evaluated the first three steps of Fig. 6, that is, the period during which water would be released and concentrated. The ultimate diameter to

which the shell would expand would be dependent on several factors, and it would not stop at the point of breakthrough to the martian atmosphere.

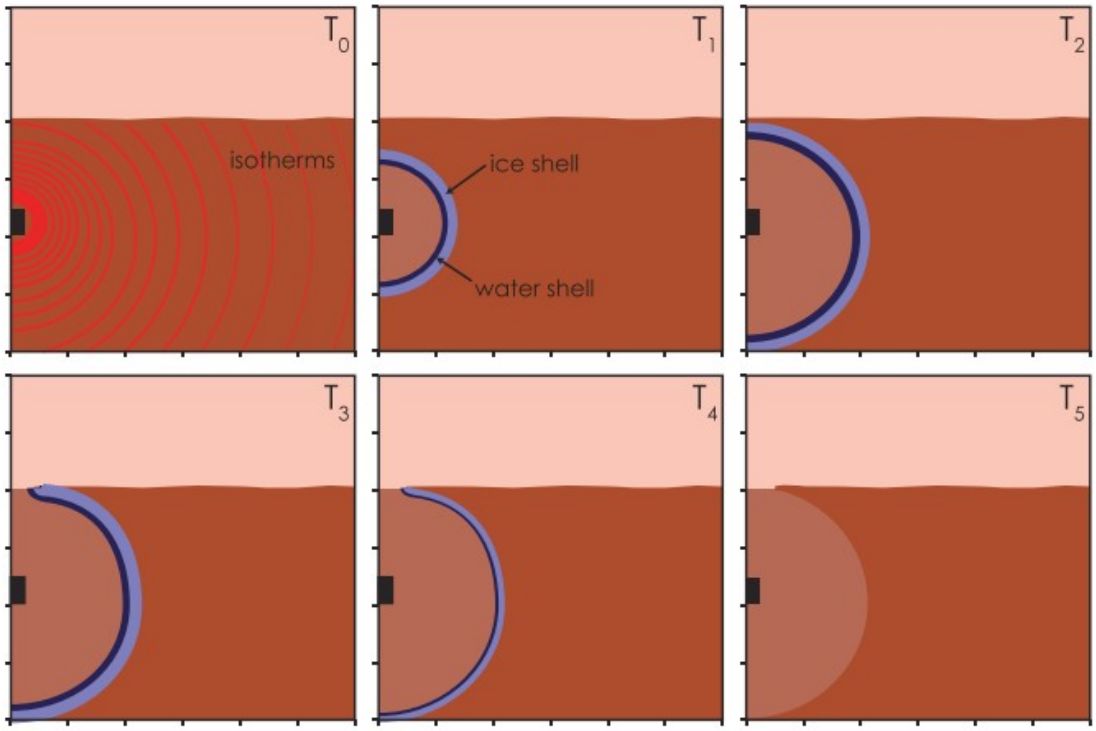

FIG. 6. Schematic cross-sections showing the general evolution in time (from T_0 = earliest to T_5 = latest) of the water and ice shells around the embedded 250-W GPHS module (black rectangle). The numerical models in this analysis cover only the periods T_0–T_2. In T_3, the water and ice shells would stop expanding at approximately 8–9 cm beneath the surface of the regolith, and they would begin to evaporate and sublimate, respectively, to the atmosphere at this depth. At T_4, the water shell would have fully evaporated, but the ice shell would continue to sublimate. At T_5, steady-state heat flow through the regolith means that a dehydrated zone would remain close to the embedded GPHS module, whereas the water and ice shells would be gone.

7. Quantitative Results of the Models

7.1. Terminology

Much of the latter discussion relates to fluid flow in porous media. Here are some definitions used throughout:

- Total porosity is assumed to be 37% in this model (a standard value for undisturbed regolith).
- Saturation, as used in problems of fluid flow in porous media (most notably in the oil industry), refers to the fraction of the pore volume that is occupied by a specific phase, usually a fluid.
- In this case, the pore network is occupied by some combination of three phases (two of which are fluids, and one of which is a solid): liquid water (S_{liq}), ice (S_{ice}), and air (S_{air}). An important constraint is that $S_{liq} + S_{ice} + S_{air} = 1$, since all of the fractions add up to unity. (In classic petroleum flow problems, the pore network is also occupied by some combination of three phases [water, gas, and oil], but in that case, all

are fluids) A conventional assumption in evaluating questions of fluid flow in porous geological materials, and that we have made in this study, is that the solid part of the soil/rock does not change—the essence of the problem is interpreting the changes in time and space within the total pore volume.

7.2. Size, configuration, and state of the water and ice shells

The system being modeled is one in which no water would be added, but instead water would be progressively and systematically redistributed within the heated zone (Figs. 5 and 6). The water would migrate outward from the heat source, creating a dehydrated zone, surrounded by water-bearing and ice-bearing shells. The water could flow in response to two forces: (1) martian gravity and (2) the pressure gradient that develops, as the heated gas in the vicinity of the heat source drives out the mobile fluids (gas and water) via advection and diffusion. The system would be open to the top, and there is a possibility of a water vapor loss to the atmosphere if all the following five conditions are met: (1) The ice and water shells reach the ground surface, (2) the presence of liquid water and ice do not render the regolith at the surface impermeable, (3) there is a sufficiently large driving force (*i.e.*, pressure) to cause vapor flow, (4) there is a sufficiently large water vapor mass in the dry zone, and (5) the temperature in the vicinity of the surface is sufficiently large to allow nontrivial sublimation. If these conditions are met, vapor will only accumulate as ice at the edge of the ice shell (advancing because of continuing heating) and vapor loss to the atmosphere will be negligible. Under the conditions of this study, water vapor losses to the atmosphere would be low, because (1) the temperature of the martian atmosphere is constant and very low, thus not permitting extensive sublimation, and (2) the mass of available water is limited, as it originates exclusively from the thermal decomposition of the minerals (the regolith is assumed to be ice-free at the time of the burial of the Radioisotope Thermoelectric Generator [RTG]).

The purpose of modeling was to place quantitative constraints on the key parameters of time, distance, mass, and water concentration. The system modeled is dynamic—it would continually change with time until the thermal anomaly has been erased and the previous equilibrium has been restored. The full lifetime of the thermal source was not modeled here due to computational resources, but it was modeled to the extent that assessments could be made regarding the system behavior and lifetime. It is beyond the scope of this article to describe in detail all of the numerical results that this model generated. The example output from the primary model is shown in Fig. 7, which shows in cross-section the distribution of water saturation (S_{liq}) and ice saturation (S_{ice}) after the model had reached a time of 10 sols. At this point, the zone in which water and ice were stable was each about 3-cm thick, and by means of advective and diffusive transfer, they were positioned at a distance of about 30 cm from the heat source.

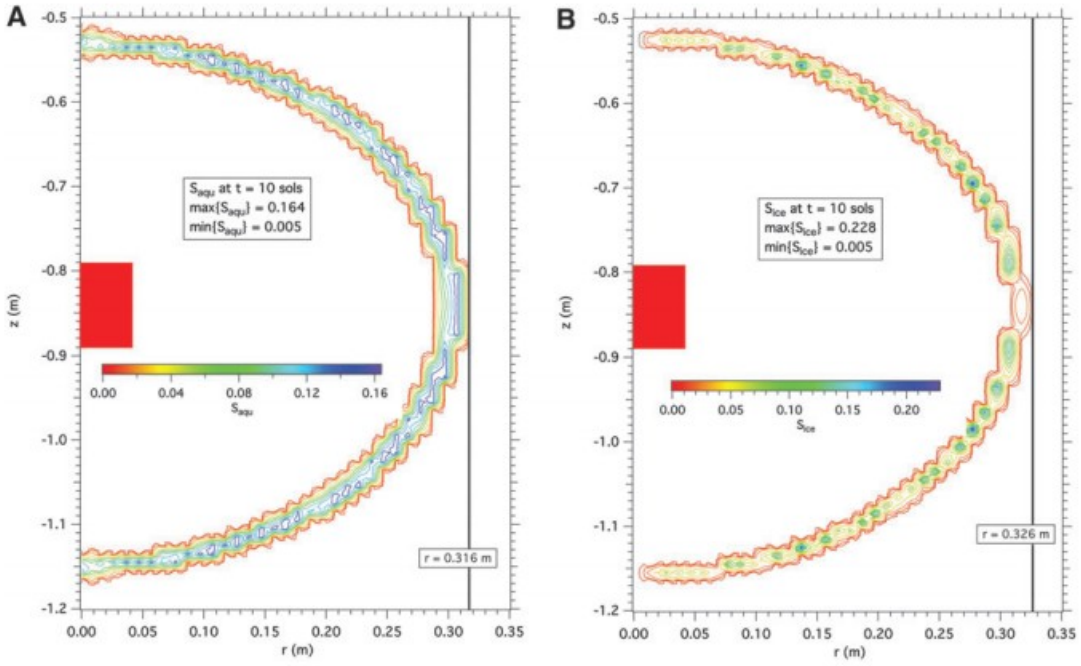

FIG. 7. Examples of the output from the primary model—these show the **(A)** water saturation, S_{aqu}, and **(B)** ice saturation, S_{ice}, at time = 10 sols. These are plotted as a cross-section, and the heat source is shown by a red rectangle. The first three contour lines in both figures are: 0.005, 0.01, and 0.02, and afterward increase by 0.02 until the max value is reached. As heat slowly diffuses away from the source, water vapor would be released by the dehydration of hydrated minerals, such as allophane and perchlorate. The water vapor would flow (because of advection caused by pressure differences, and diffusion fueled by concentration differences) outward and condense and solidify in the pore network of the regolith.

In the primary model, at a model time of 50 sols, the outer limit of the water shell had reached a radius of about 0.6 m, the outer limit of the ice shell was at 0.9 m, the water shell was about 20-cm thick, and the maximum value of S_{liq} within the liquid water shell was 0.154. At a model time of 200 sols, the outer limit of the water shell was at a radius of about 1.1 m, the outer limit of the ice shell was at 1.7 m, the water shell was about 30-cm thick (the appreciable shell would be ~10-cm thick), and the maximum value of S_{liq} within the liquid water shell was also 0.154. In at least some cases, the ice saturation would be substantially higher than this, and this model indicated values of S_{ice} as high as 0.89. Note that there can be no water vapor loss to the atmosphere if the sum $S_{liq} + S_{ice}$ is close to 1 because then the combined ice and liquid water shells are impermeable to gas flow.

The primary model shows that beginning at about 30 sols, heat from the system would start reaching the atmosphere (Fig. 8). By a time of about 200 sols, the conduction of heat to the atmosphere would be about 60 W (about a quarter of the heat output of the RTG), and by 300 sols, it would increase to about 90 W. Even though we did not run the numerical model beyond 300 sols, we can expect that the rate of heat loss would continue to increase until it matched that of the heat input from the RTG, at which point the system would be at a quasi-steady state (given the very long half-life of Pu—in reality, a very slow decline would begin once the maximum heat loss is

reached). Thus, although the model had not yet reached steady state by 300 sols, the heat flow in and heat flow out were rapidly approaching balance. The maximum horizontal extent of the ice boundary at 200 sols, the time of stalled vertical ice front growth, was ~1.7 m in radius; minor further growth is expected with increasing loss to the atmosphere. This was also confirmed in the secondary model.

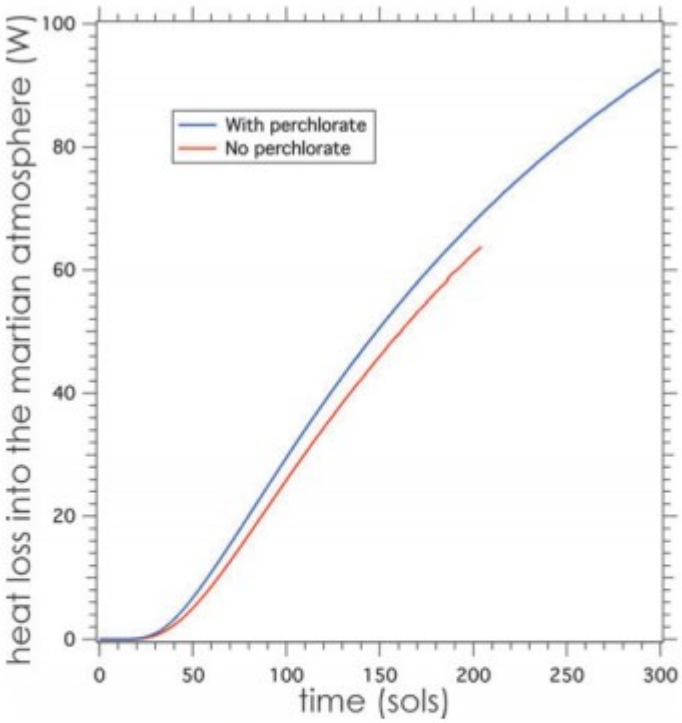

FIG. 8. Modeled loss of heat into the martian atmosphere (in watts) as a function of time during the first 300 sols of the scenario. By 300 sols, 37% of heat being released by the nuclear source (250 W) would be lost to the atmosphere. The figure shows results from both the ''with perchlorate'' and ''without perchlorate'' cases, and they show only minor differences. The perchlorate cases would have higher water content and thus higher conductivity.

By an elapsed time about 50 sols, the primary model shows that the ice shell would be close enough to the surface that it would start being affected by water vapor loss via sublimation to the atmosphere (Fig. 9). This would begin to slow the growth of the ice shell in a vertical direction. By the time of our primary model run at 200 sols, the rate of vertical growth slows dramatically, and most of the expansion of the ice shell happens laterally, although slowly. However, since the primary model did not take into account the diurnal temperature fluctuations in the upper 10 cm or so of the regolith, we cannot quantify the evolution of conditions in the uppermost regolith. The secondary model indicated that the maximum height of the ice shell was still >20 cm away from the surface, and under the conditions modeled, liquid water would be unstable above that.

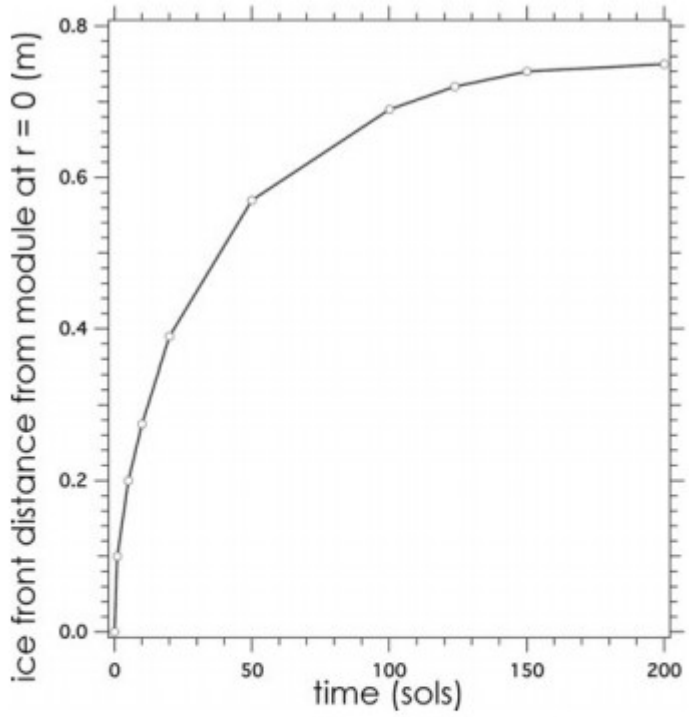

FIG. 9. The position (in meters) of the top of the ice front directly over the heat source, from the primary model, as a function of time. Note that by 150–200 sols, the rate of change has slowed dramatically, reflecting the loss of water vapor and ice by means of sublimation to the atmosphere. Separate calculations (Section 6.2.2) show that the top of the ice would not advance any further than about 0.8 m on this scale, due to vapor diffusive equilibrium with the atmosphere.

7.3. The thermodynamic activity of water in the water shell

The water activity (a_w) would be affected by both matric effects from the electrostatic forces between the water and the solid surfaces and solute effects from dissolved salts, most particularly perchlorates (*e.g.*, Marion *et al.*, 2010). Both factors affect the strength of the chemical bonds affecting the water molecules. Whether the water would be biologically available would depend on whether organisms could overcome the strength of these inorganic bonds (Potts, 1994).

7.3.1. Matric effects on water activity

As recently summarized by Rummel *et al.* (2014), loss of water in a system dominated by one or more solid surfaces, that is, decrease in matric water potential or water activity, exemplified by desiccation of a porous medium (soil, martian regolith, food, etc.), is more inhibitory to microbial activity than equivalent decreases in water activity (a_w) caused by solutes such as NaCl or sugars (Harris, 1981); however, strongly deliquescent salts such as perchlorates, as discussed later, have a much larger effect. As a porous medium loses water during desiccation, the thickness of water films

diminishes. Water film thicknesses vary primarily as a function of water potential (or water activity), but they are also influenced by surface roughness, surface hydrophobicity, temperature, texture, and other factors; water film thickness are also not uniform, so an average water film thickness is measured or calculated (Harris, 1981; Papendick and Campbell, 1981; Tokunaga, 2012).

In experiments using bacteria-laden Earth soils, respiration (carbon dioxide production) can easily be measured, and it is a sign of microbial metabolism. In desiccation experiments, carbon dioxide production diminishes to nondetectable levels when soils are dried to the point that a_w is about 0.9. The fact that metabolism of the microbial community ceases at this point does not mean that they have all died—many microbes have strategies for going dormant; however, it does mean that active processes, including reproduction, have ceased. As per the data presented in Rummel *et al.* (2014), a water activity of 0.9 is approximately equivalent to an average thin film thicknesses of about 15 nm or less. Actual water film thickness varies with a number of parameters, including surface roughness, surface hydrophobicity, solutes, temperature, etc.

In the relationship between water saturation and thin film thickness, there is a strong dependence on grain size, since the smaller the grain size, the greater the surface area. For a water saturation of 0.15 (the maximum predicted by the numerical model), the thin film thickness would be lower than the threshold value of 15 nm only for soils with an average grain size lower than about 0.5 µm. This is exceedingly fine-grained. In addition, there is also a strong dependence of thin film thickness on mineralogy, since different minerals have different specific surface area. However, except in very clay-rich regolith, the effect of specific surface area is typically relatively small. We know that in many places (*i.e.*, locations where the missions MER, PHX, MSL, and Viking have visited) martian regolith has an average grain size that is significantly larger than the 0.5-µm threshold mentioned earlier; in many examples of martian regolith, the constituent components are composed of rock fragments, and the igneous minerals feldspar, pyroxene, and olivine, all of which have low specific surface area.

7.3.1.1. Conclusion

There is likely to be some regolith on Mars for which the water film thickness at $S_{liq} = 0.15$ would be <15 nm (*i.e.*, too thin for microbial reproduction). However, we cannot conclude that this would be true of all regolith (we know that coarser-grained variants exist). There is no way of selecting a landing site for which the matric-induced effects on the reduction of water activity would be an argument against Special Regions conditions at the scale of a Mars landing ellipse.

7.3.2. Solute effects on water activity

In the design of this numerical simulation, we were aware of the potential effect of Ca-perchlorate (and other similar compounds) in lowering the freezing point of water. If such solid materials were present in the regolith in which the water shell develops, it could be dissolved when water is present, and then reprecipitated as the liquid water evaporates. To understand this process better, some parts of the numerical model were run both with and without perchlorate.

In the runs without Ca-perchlorate, the system was initially assumed to contain anhydrite (0.9 wt %; see Table 1), and gypsum was allowed to form. For cases with initial liquid saturations <0.02, water uptake by gypsum precipitation causes discontinuity in trends followed by dryout. In the runs with Ca-perchlorate, the concentration was assumed to be 1.5 wt %, which is believed to be a plausible upper limit. Based on the simultaneous release of HCl and O_2 in the SAM experiment, combined with APXS Cl concentration data, the rocks in Gale Crater are interpreted to contain variable amounts of Cl_2O_7 (up to 1.3%) (Ming *et al.*, 2014). The perchlorate content of the regolith at the PHX landing site is 0.4–0.6 wt % (Hecht *et al.*, 2009; Kounaves *et al.*, 2010), but there are no data to correlate the chemistry of polar regolith with that of low-latitude regolith. In addition, there is no information about the concentration or distribution of perchlorate elsewhere on Mars, since it cannot be detected from orbit.

The water activity as a function of evaporation (from heating) was computed by using TOUGHREACT-Pitzer (Zhang *et al.*, 2006), and Pitzer ion-interaction parameters from Wolery *et al.* (2004) were augmented by the data of Marion *et al.* (2010) for perchlorates. The simulations involved evaporating solutions in contact (and not) with calcium perchlorate, assuming a range of initial liquid saturations, starting at 4°C under martian atmospheric pressure. Results are shown in Fig. 11 for water activity versus liquid saturation in cases with and without Ca-perchlorate. In the runs without perchlorate, there would be essentially no reduction in the water activity below that of pure water (1.0) over most of the relevant range of liquid saturation. When Ca-perchlorate is added to the model, solute-induced effects reduce the water activity significantly, to values down to about 0.5. However, we should also note that perchlorate is chaotropic (Cray *et al.*, 2013a), and chaotropic solutes limit biological activity even further than would be evident from a consideration of the solute-induced decrease in water activity alone (Cray *et al.*, 2013b).

7.3.2.1. Conclusion

For perchlorate concentrations between 0 and 1.5 wt %, a geologically plausible upper limit, the solute effects on water activity are not sufficient to drive conditions of T and a_w inside the water shell out of the “habitable” zone defined by Rummel *et al.* (2014). Since perchlorate cannot be detected from orbit, we have no way of knowingly avoiding a landing site that has Ca-perchlorate concentration in this range. Thus, it cannot be ruled out that

perchlorate present in very small quantities could increase local water released by a thermal source to a water activity level that is marginally conducive to biological activity. Models that include perchlorate, hence, are bounding cases.

7.4. Results from the secondary model (Sierra-Aria)

Figure 10 illustrates the results from the secondary model. The models agree with the rapid development of the ice dome around the GPHS. At 10 sols, both models have an ice dome that would reach ~0.35 m from the surface. T+RGB has a liquid saturation of 16.4%, and Sierra-Aria has a liquid saturation of 16.8%. After 50 sols, the model outputs begin to disagree noticeably. The primary model is 5–10 cm closer to the surface, and it exhibits 15.5% liquid water saturation versus 8.45% in the secondary model. At 200 sols, both ice domes slow their advance; the primary model comes within 10–20 cm of the surface, whereas the secondary model indicates that the ice dome advances only 1–2 cm closer to the surface than at 50 sols. Also, the primary model at 200 sols has a liquid water saturation of 15.5%, whereas the secondary model is nearly completely ice, with a liquid water saturation of only 1.2%. The Sierra-Aria simulation was continued to 500 sols. The liquid water disappears completely after 400 sols. The ice continues to disperse upward, and it reduces to a saturation level of 3.2% by 500 sols. The secondary model agrees qualitatively with the mechanism that forms the ice dome trapping a thin layer of liquid water. This agreement is robust at 10 sols, but the secondary model begins to indicate less transport and less liquid water at 50 sols and later. At 200 sols, when the primary model exhibits liquid water close to the surface, the secondary model is nearly all ice, and well away from the surface. The difference appears to be due to the temperatures of the two models near the surface. The secondary model temperatures at the surface never exceed 212 K during the daytime, which does not support liquid water at martian atmospheric pressure.

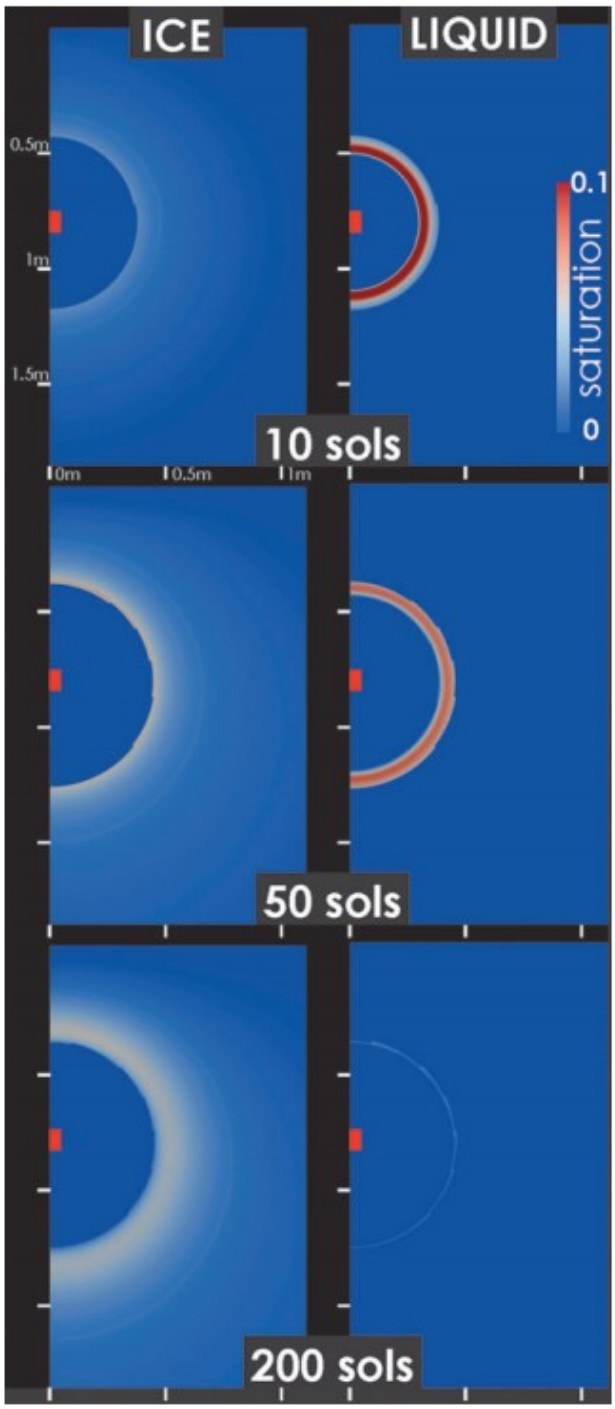

FIG. 10. Results from the secondary model (shown in cross-section; scale is labeled on the upper left figure), which included diurnal and seasonal surface variations. Liquid saturations are comparable to those in the primary model, although lifetime of the water was less than derived by the primary model, which assumed isothermal boundary conditions. The secondary model shows no water present after 300 sols (ice only). The extent of the ice and liquid boundaries are bounded within those of the worst-case primary model.

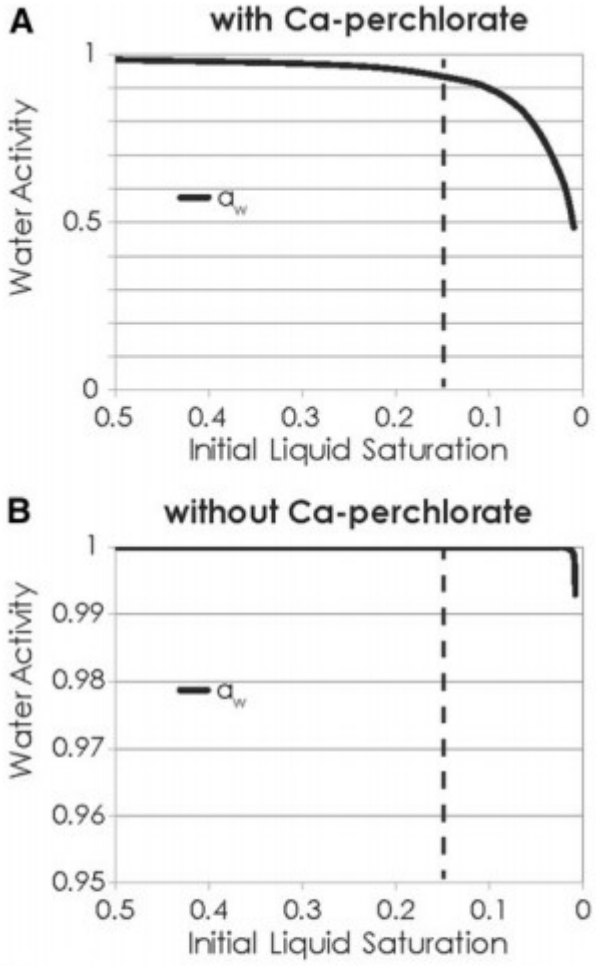

FIG. 11. Comparison of calculated water activity with and without Ca-perchlorate, from the primary model. The maximum liquid saturation of about 0.15 found by this numerical model is shown by the vertical dotted line, and saturations from that value down to zero would be present at different times and places within the modeled volume. The calculated water activity is shown by the blue lines. Without perchlorate (Case **A**), the water activity would be essentially 1.0 over most of the range of liquid water saturations found. With perchlorate (Case **B**), the water activity would be significantly reduced (note the change in scale of the two figures), and it would be approximately 0.5–0.95 over the range of water saturations of interest. However, note that these calculations take into consideration only solute effects on water activity, and not matric effects.

The secondary model was also used to study the sensitivity of the results to the assumed physical properties and boundary conditions. As part of this sensitivity analyses, the mesh size was varied, and the diameter of the mesh was increased to 5 m as a result. The size of the mesh was found to be a significant effect, with smaller mesh radii leading to higher temperatures

near the surface, enough in one case to support liquid phase at the 200-sol radius. The effect of the diurnal thermal boundary condition and the presence of gravity were also examined. The thermal condition at the top surface, either a diurnal variation or an isothermal condition, had an intermediate effect. An isothermal assumption increased the water dwell time in comparison to a diurnal variation.

In summary, the secondary model confirms the qualitative behavior of the primary model early in the simulation, but it indicates that a pure ice-only dome remains after several hundred sols. It, thus, supports the original premise of the primary analysis as being conservative.

7.5. Could/would the liquid water flow?

An S_{liq} value of 0.15 would imply the presence of water as thin films on all mineral surfaces, and possibly also additional “free” water in the pore bodies, depending on the specific surface area of the regolith. The point of distinguishing these two types of water is that thin films are not free to flow because of the electrostatic forces associated with the highly charged mineral surfaces, but larger blebs of water in the pore network do have the potential to flow from one pore to another. This point is illustrated by an example pore network (Fig. 12). The total pore volume consists of pore bodies that contain most of the pore volume and that are separated by pore throats. The points of greatest restriction in the pore throats are labeled pore necks. Whether the water would or could flow from one pore body to an adjacent one is a complex question, and it depends strongly on the nature of the pore throats and necks, the quantity of available water (S_{liq}), dissolved salts (which affect the electrical properties of the water), and pressure conditions. However, in this case, the liquid water saturation is relatively low (in comparison to many other fluid flow problems in porous media to which this modeling capability has been applied); and in our primary model calculations, the force of martian gravity is insufficient to cause macroscopic water movement. Had the water shell reached full water saturation, some water pooling at the bottom of the water shell might have been plausible, but in any case, this water could not have flowed further downward into the underlying very cold (183 K) regolith/rock without freezing first.

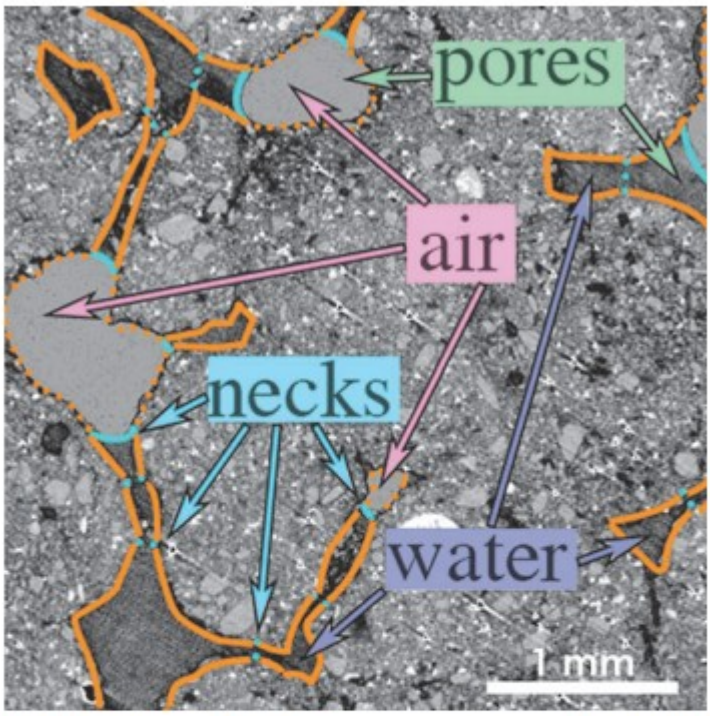

FIG. 12. Example of the pore network in a rock (modified from Xu and Louge, 2015). Note that in this illustration, the pore network is partially occupied by water, and partially occupied by gas. The pore necks (also called pore throats) are the points of constriction between adjacent pores; their size is a primary driver on permeability. A 1-mm scale bar is included in the bottom right of the image. (The original CT image is captioned to describe the pore wettable surface area [orange] and neck area [blue], with continuous and dotted blue lines showing air–water interfaces and boundaries between connected water-filled pores, respectively.) CT, computed tomography.

This conclusion was further tested by turning gravity on/off in the secondary model. We questioned whether there was a noticeable difference in behavior, possibly indicating flow. We did see a minor shape effect, implying that some small downward movement of the liquid water may be possible under some conditions, but this movement may also have resulted from minor differences in thermal and pressure gradients (heat flow above vs. below the thermal source).

7.5.1. Conclusion

Our models clearly show that at the very low water saturation levels implied by this scenario, the force of martian gravity would cause either no or, possibly, minor liquid water movement within the volume that is heated above the melting point of water. However, liquid water flow through the underlying and surrounding very cold (183 K) regolith/rock would be impossible because the water would freeze; likewise, flow across the inner

surface of the water shell would not occur because the water would evaporate (Fig. 13). Thus, regardless of the outcome of the calculations related to fluid flow in porous media, the liquid water formed in the water shell would be trapped by thermodynamic boundaries that would prevent its movement.

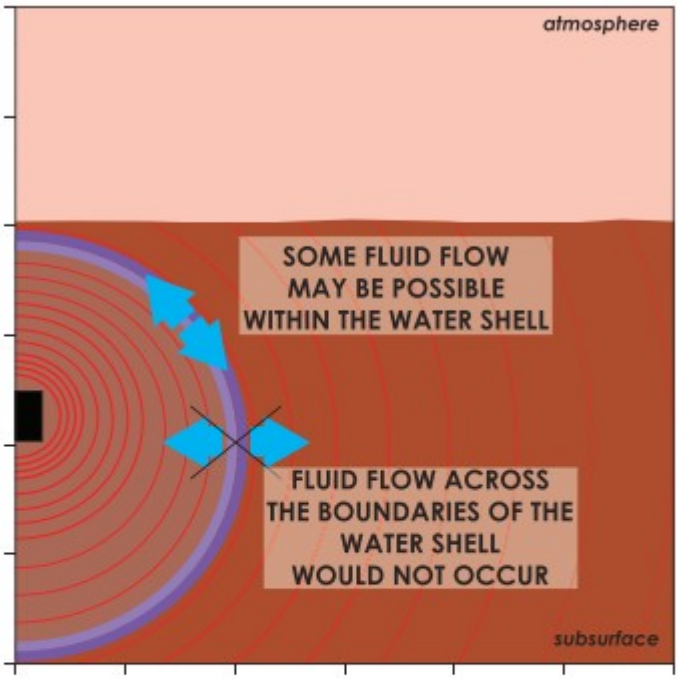

FIG. 13. Schematic cross-section showing the potential for liquid water flow within the thermal anomaly, at the time that water is most concentrated. Flow across the boundaries of the water shell would be thermodynamically impossible, because the water would either freeze or evaporate—it would not be able to stay in liquid state. However, we were not able to determine whether fluid flow within the water shell would occur under the conditions assumed.

7.5.2. Overall conclusion

For periods of time, it is plausible that conditions may be present that meet the definition of induced Special Region as a result of an embedded thermal heat source.

7.6. Probability of microbial survival and dispersal

As described in sections 7.3.1.1 and 7.5.2, it is possible that organisms could be present in the liquid water shell, for some times and positions, and depending on the species present, may be capable of reproduction during these time windows. Therefore, to address the second part of our problem statement, we must consider whether there is a transport mechanism through which introduced terrestrial organisms could be mobilized to naturally occurring Special Regions elsewhere on Mars.

7.6.1. Impact-related dispersal

One of the only mechanisms for the dispersal of a possible amplified set of microbes from the system would be a direct hit by a bolide that is large enough to throw the material to some distance. The same sort of risk exists for a meteorite strike on a rover, except in the subsurface case we are considering, the community could have grown. This would require that the incoming bolide impact a specific 5-m-diameter region of Mars (the approximate diameter of the heated zone) within ~500 years of a spacecraft crash (the time until the radioactive heat source decays). This probability can be estimated by using the following six-step calculation (courtesy of Dr. Nadine Barlow):

(1) The current crater production rate for craters $D \geq 3.9$ m (Daubar *et al.*, 2015) $= 1.8 \times 10^6$ $D > 3.9$ m/(km^2·year)

(2) Area of circle with radius 2.5 m $= 1.963 \times 10^{-5}$ km^2

(3) Calculated number of craters $D > 3.9$ m formed in a 5-m diameter circle on the surface of Mars in 500 years: # $= (1.8 \times 10^6$ $D > 3.9$ m)/(km^2·year) $\times$ (1.963×10^{-5} km^2) $\times$ (500) $= 1.7667 \times 10^{-8}$ craters

(4) Surface area of Mars $= 1.443 \times 10^8$ km^2

(5) Number of craters $D > 3.9$ m formed over entire surface of Mars in 500 years: # $= (1.8 \times 10^6$ $D > 3.9$ m/km^2 yr^{-1}) $\times$ (1.443×10^8 km^2) $\times$ (500) $= 1.2993 \times 10^5$ craters

(6) Probability that an impact of the right size would strike a particular 5-m diameter circular region on Mars in the next 500 years: P $= (1.7667 \times 10^{-8}$ craters)/(1.2993×10^5 craters) $= 1.36 \times 10^{-13}$

To estimate the probability that the ejecta would be delivered to a martian Special Region, we would need to reduce what has just been stated by additional probability factors that would be dependent on the position of the landing site relative to the Special Region and certain mechanical attributes

of the target. We would also need to consider the probability that the microbes could survive the force of impact and not be vaporized or succumb to excessive temperatures and pressures, and would arrive at their new home not only in a viable state but also prepared to reproduce. However, none of these can be estimated in a general way that is not site-specific. Suffice it to say that the resultant probability would be another order (or orders) of magnitude less than the probability of a strike alone.

7.6.2. Transport by entering a water table

One of the primary objectives of the SHARAD and MARSIS radar instruments on MRO (2005) and MEX (2003), respectively, has been to search for a martian water table. Although Clifford *et al.* (2010) have persuasively argued that subsurface water must exist at some depth on Mars, the magnitude of that depth has been difficult to estimate, and we have sought a direct measurement by means of the radar surveys just cited. There are two important aspects of the data collected to date:

(a) Where radar coverage exists, no reflections from a water table have been detected (Plaut, 2014). The martian subsurface attenuates the radar energy, and below about 400 m depth, the radar reflections from small geological features become so weak that we no longer have confidence that the data can be interpreted. The radar energy simply disappears into the subsurface and never comes back.

(b) These two radar datasets have yet to be completed at a planetary scale. However, by 2014 (and as summarized in Rummel *et al.*, 2014) the picture had filled in enough that there were no regions of meaningful size that had not been covered. Those maps are even more complete as of this writing in 2017, and still no water table has been detected.

Thus, it is now possible to conclude safely that there is no water table within 400 m of the surface at any place on Mars, and specifically below any candidate Mars 2020 landing site. The actual distance to a water table may be many times larger than that.

In addition, the temperature of the ground before impact of the MMRTG would be far below the freezing point of water (assumed for the purpose of numerical modeling to be 183 K, although more plausible values for potential Mars 2020 landing sites might be 215–225 K) (Appendix 1). As quantitatively determined by the model, any water vapor generated by the decomposition of hydrous minerals would diffuse outward, condense to liquid, and finally freeze to ice when it interacts with the cold surrounding country rock/regolith. This also applies to transport downward, toward a potential water table. Once the temperature drops below the freezing point, transport of liquid water (and any potentially entrained microbes), as well as meaningful quantities of water vapor, would stop. Although small amounts of highly concentrated brine could be produced by the deliquescence of certain trace minerals, and this brine, in its most concentrated form, could remain

liquid at the temperatures listed earlier, this brine would be progressively diluted by the water generated by mineral decomposition and transported as water vapor. It would not be possible for such brine droplets to maintain their salinity and to coalesce into a large enough mass to generate the hydraulic head that is necessary to flow through the porous medium.

7.6.3. Dispersal by wind

The scenario we have modeled is one in which the system is not closed—it would be open to the atmosphere at the top. Once the water vapor generated by mineral decomposition reaches the upper surface of the regolith, it would diffuse into the atmosphere, mix with it, and be lost to the system being modeled. Could a microbe somehow make it to the surface in this scenario, and then travel from the impact site to a nearby Special Region by means of the wind?

One of the conclusions of the primary numerical model is that mass transfer within the thermal anomaly would happen by means of the movement of water vapor. The water vapor would be a mobile fluid, and it would move by pressure gradients: As heated gas in the vicinity of the heat source expands, it drives out the mobile fluids by advection and diffusion. The water that would be in the ice shell would be incapable of movement because it would be in a solid phase. The fact that the ice shell would progressively expand during the early phases of this scenario would be a result of heating of its inner surface to a temperature above the local frost point, diffusion of water vapor to the outer surface, and finally recrystallization. As described earlier in Section 7.4, we can conclude that liquid flow across those two surfaces would not be possible for reasons of simple thermodynamics; though much of the water in this zone would be present as thin films on the mineral surfaces, at water saturation values of up to 0.15, we cannot conclude that short-range flow would be impossible (Section 7.4). What we can conclude, however, is that this flow, if it happens at all, would be restricted to the interior of the water shell and run parallel with it, and not perpendicular to it.

As discussed earlier in Section 6.2.2, at the candidate Mars 2020 landing sites, the atmosphere is undersaturated with respect to water vapor at all times of day (we have no evidence that either frost or dew forms at these latitudes). Thus, any water vapor that diffuses into the atmosphere would reduce the degree of local undersaturation temporarily; however, since the atmosphere is well mixed on the timescale of this problem, and has a much larger capacity, it would behave as an infinite heat and water vapor sink. Thus, in the upper part of the system, where ice would be in diffusive equilibrium with the atmosphere, the water shell would be unstable with respect to vapor down to some depth below the surface, and vapor would be systematically lost. Neither the water nor the ice shells would make it to the surface.

Terrestrial microbes cannot travel by vapor diffusion. Therefore, there would be a limit to how close they would be able to get to the surface, as the only

pathway for mass movement to the ground surface in this system would be vapor diffusion. Thus, we conclude that any microbes present would be separated from the water by this process, and they would not reach the surface where they could be picked up by the wind.

7.6.3.1. Conclusion

Three possible mechanisms for the movement of potentially present microbes out of the thermal anomaly have been evaluated. Two of them, liquid water flow downward to a water table and liquid water flow up to the surface, have been found to be thermodynamically impossible. The third, a direct meteorite strike and impact-related delivery of microbes from the thermal anomaly to a nearby Special Region, would be possible, but its probability would be vanishingly low ($<10^{-13}$).

8. Discussion

8.1. The possibility of Special Regions thermodynamic conditions

Could liquid water exist in the subsurface? Given the starting and boundary conditions assumed for this model, we conclude that within the water shell, the currently accepted a_w and T constraints for Special Regions (Rummel *et al.*, 2014) could be satisfied temporarily. Results from the secondary model, including the increased exchange with the atmosphere, indicate that the water shell would largely disappear by ~300 sols (sublimation and repeated evaporations). Note that since the zone that would be heated moves with time, there would be no specific places within the thermal anomaly where the combination of conditions would be exceeded for this entire time. This takes into consideration both the matric-induced and solute-induced effects on a_w (Section 7.3). Thus, within the water shell, we cannot use the known limits in T and a_w on microbial reproduction to argue that cell division would be impossible.

Could liquid water exist at the martian surface above an anomaly of this type? There have been multiple studies over the past four to five decades looking at whether liquid water could persist at the martian surface under natural conditions. Issues examined have included the stability of surface water against evaporation (*e.g.*, Ingersoll, 1970; Hecht, 2002), natural heating rates and potential for melting of buried ice (*e.g.*, Mellon and Phillips, 2001), the combined effects of boiling and evaporation (*e.g.*, Haberle *et al.*, 2001; Richardson and Mischna, 2005), brines (*e.g.*, Brass, 1980, Sears and Chittenden, 2005), and the lifetime of channelized water versus flow velocity (*e.g.*, Carr, 1983; Heldmann *et al.*, 2005). In the past 10–15 years, the interest in this topic has increased in response to the discovery of gullies and the recurring slope lineae (Malin and Edgett, 2000; McEwen *et al.*, 2011).

A common issue in modeling these effects is that the current martian atmosphere is very dry. Even at the equator where surface temperatures sometimes do exceed 273 K, water would not persist in a condensed phase—it would evaporate. Generally, under natural conditions, ice sublimes faster

than it can be warmed to melting. To find conditions where some amount of liquid water would be stable, if only briefly, various researchers have tried to invoke special scenarios such as brines (to reduce the vapor pressure), springs and seeps (to rapidly force liquid water from a subsurface aquifer), and high obliquity (to raise the atmospheric humidity and suppress sublimation). Although some researchers have attempted to argue for meta-stable or transient liquid water under atypical natural conditions in some locations, these conditions would not apply to potential Mars 2020 landing sites, since that would have resulted in them being identified as Special Regions and being excluded from selection. Thus, this study of unnatural conditions is consistent with the body of previous studies of natural conditions—surface and near-surface water and ice would transition to vapor too fast to persist at the surface at a Mars 2020 landing site.

8.2. Considerations related to the biological potential

8.2.1. The effect of desiccation

Whether or not microbial reproduction would happen depends on many factors beyond T and a_w. Within the water shell, there may initially be nutrients present (either native to Mars or injected along with the impact event) that could sustain the microbes until the supply would be exhausted. There would be no mechanism for resupply of nutrients to the water shell, which would limit microbial lifetimes. In addition, the water shell would be temporary, because the water would evaporate over time—this also limits microbial life expectancy.

What happens to terrestrial soil microbes under extreme desiccation? Microbes can happily live in conditions where the water is present as more than just thin films. This gives them the opportunity to move, and if the water flows, the water can bring nutrients to them. However, with increasing desiccation, at a film thickness of less than approximately 10–20 nm, the liquid medium cannot flow because of the electrostatic forces associated with the highly charged mineral grains and solute diffusion is greatly reduced (*e.g.*, Griffin, 1981). The water, thus, cannot transport nutrients or energy to the microbe. In addition, the microbe itself has lost its ability to move to acquire nutrients. In such experiments on Earth, microbial metabolism ceases at this point. Some microbes have the capacity to go dormant, for example, as bacterial endospores, but without influx of new water, cell proliferation is impossible. In our Mars case, we, therefore, infer that microbial metabolism, possibly including cell division, may be temporarily possible within the water shell. A limitation for the microbes, however, is that even if nutrients were present in the volume where the water shell forms, the absence of water flow means that no new nutrients could move in, and the microbes could not move out to seek nutrients elsewhere. In any case, in the latter parts of the scenario, the water content would decrease to thin-film levels and the microbes would starve (Fig. 14).

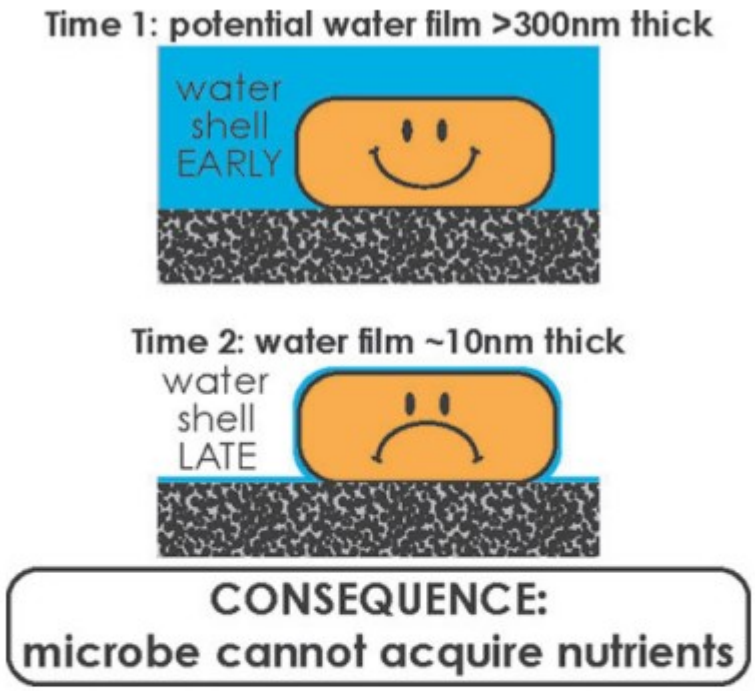

FIG. 14. Schematic illustration of a 200-nm-diameter microbe (a relatively small terrestrial bacterium) on a solid surface in an unsaturated porous medium. Water (in blue) is shown to scale relative to the microbe. Time 1 represents the early conditions when the water saturation could have been high enough to be present as relatively large blebs in the pores. Time 2 represents the same microbe, after desiccation, where the water would be present as a thin film ~10 nm thick. Diffusivity in the film would be nearly zero, and the effective viscosity would increase as the water film thinned. Under these conditions, the microbes would all starve to death.

8.2.2. Probability of reproduction

The probability of reproduction, given the existence of permissible conditions of T and a_w, would be the combined probability of the following factors (for which we have little/no basis for estimating):

- The probability that the terrestrial microbes would survive the off-nominal EDL event (and associated unplanned heating).
- The probability that the terrestrial microbes would be injected into the subsurface within approximately 2–5 m of the heat source.
- The probability that all other environmental conditions are suitable for reproduction.

8.2.3. Probability of transport out of the thermal anomaly

Finally, as discussed earlier in Sections 7.4 and 7.5, we have been unable to identify a viable mechanism for communication of the water-containing volume, and any possible contained microbes, during the time of their survival, with potentially naturally occurring Special Regions elsewhere on Mars.

8.3. Fate of potential organisms: summary

In summary, we can define four regions around the thermal anomaly for which embedded terrestrial organisms would have a different fate (Fig. 15).

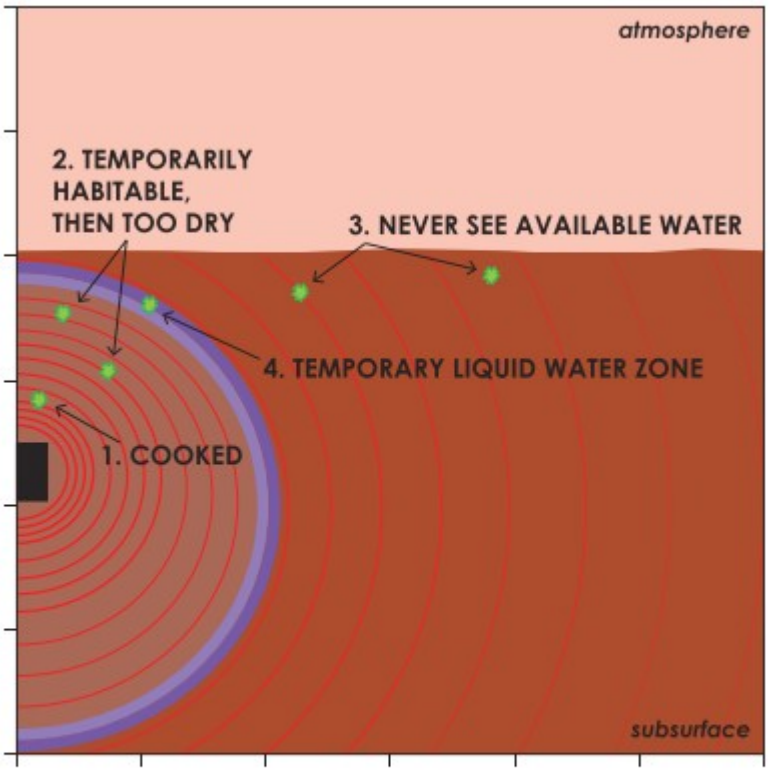

FIG. 15. Schematic cross-section summarizing the fate of microbes that may potentially be in and around the thermal anomaly. See explanations in text (Section 8.3) for further details.

(1) Organisms that were initially close to the heat source may have enjoyed conditions for a short while, later to be “cooked.”

(2) Some that remain uncooked exist with no available water source and lose viability.

(3) Organisms outside the ice shell have no access to water and are too cold for biological activity.

(4) Organisms that reside in the “quasi-stable” water zone can potentially reproduce but are trapped in rock/grain pores, and are constrained to a limited number of generations and no opportunity for dispersal.

8.4. Possible extension to other martian conditions

The regolith on Mars has properties that vary from place to place, and we do not have data on the full range of its variation. We have evaluated qualitatively the potential significance of some of those variations, but because of constraints in time and budget, were not able to quantify all of them.

For many of the parameters assumed in carrying out this evaluation, changing them would change the spatial scaling of the water and ice shells (*i.e.*, making them larger or smaller), but not the overall sequence of events, the basic geometrical configurations, the length of time that thermal anomaly persisted in the region, or the conclusions. This includes modifying the concentration and identity of the minerals in the region to be heated, the thermal conductivity of the regolith, the depth of penetration of the GPHS module, and the porosity and permeability of the regolith. For example, the assumptions made here regarding the thermal conductivity of the regolith certainly have an effect on the outcome of the model. There are many factors that have secondary effects on the thermal conductivity; however these are minor compared with the significant change in thermal conductivity that occurs when very dry martian regolith has even a small amount of water (liquid or ice) added to the system. However, if the assumptions made here were modified, and the regolith were substantially more (or less) thermally conductive, the diameter of the ice and water shells would be either larger or smaller than the baseline case modeled, and each would likely be either thicker or thinner. Note that higher conductivity results in lower local temperatures such that much of the regolith in the heat affected zone would not see high enough temperatures to release water. Higher thermal conductivity might also have an effect on the length of time that the ice and water shells persist, as they would grow more quickly to intersect the surface, and any water produced would be likely to more quickly escape to the atmosphere. An induced Special Region *sensu strictu* would still be created, but even if introduced microbes were to survive and reproduce, they would remain trapped below ground. The same considerations would apply to increasing or decreasing the concentration of hydrous minerals.

What would happen if the spacecraft impacted material with an alternate mineralogy? Gypsum, for example, has a significantly higher water content than the three hydrated minerals assumed in this study (perchlorate, allophane, opal). Similar to the earlier discussion, we hypothesize that this would not change the essential behavior of the system as it relates to Special Regions; however, it very likely could change the rates and scaling factors.

8.5. High-level conclusion

Embedding the heat sources for the MMRTG into the martian subsurface can create a local environment that: (1) would temporarily satisfy the conditions for a martian Special Region that is conducive to terrestrial organism reproduction (for more than 300 sols), but (2) no mechanism has thus far been identified that would provide a transport mechanism through which introduced terrestrial organisms could be mobilized from this “induced” Special Region to naturally occurring Special Regions on Mars.

Acknowledgments

This work was publicly presented at the AbSciCon conference in April, 2017 (Shotwell *et al.*, 2017). Discussions with, and feedback from, a number of members of the scientific community are gratefully acknowledged, and they have been incorporated into the logic of this analysis. In particular, the authors thank Sylvain Piqueux for help with modeling the thermal environment, Nadine Barlow for help with the cratering calculations, and Jeff Plaut for interpretations of subsurface water on Mars. Discussions early in this study with Melissa Jones, Cassie Conley, and Nick Benardini on planetary protection matters, and with Doug Bernard regarding the Mars 2020 mission, were very helpful. For five of the authors (Shotwell, Hays, Beaty, Peterson, and Goreva), government sponsorship is acknowledged. The perceptive thoughts of two reviewers are gratefully acknowledged. The research was carried out at the Jet Propulsion Laboratory, California Institute of Technology, under a contract with the National Aeronautics and Space Administration. This document has been cleared for Unlimited External Review: URS265787.

Appendix 1

Summary of Inputs to the Models

Our best data on the regolith mineralogy, porosity/permeability, and grain size distribution are from the instruments on Mars Science Laboratory (MSL). Although the regolith is different in various places, the specificity of the MSL results provides a credible starting point for inputs to the models. Sensitivity to variations in mineralogy or mineral concentration, to encompass other parts of Mars, was evaluated qualitatively, but not quantitatively. Where direct martian data were unavailable (*e.g.*, the enthalpy of Ca-perchlorate), terrestrial analogs were used, though estimates were required for some

reactions where no data exist. In the following sections, we summarize the primary input parameters, and our rationale for making these assumptions.

Input parameter: regolith water content

For water content of the regolith, neutron data collected by Dynamic Albedo of Neutrons (DAN) along the pathway driven by MSL were used. This instrument collects measurement of total hydrogen (modeled as “water equivalent hydrogen” or WEH) over a 3-m-wide, 60-cm-deep footprint. Although the single highest WEH modeled from the DAN data was 10%, due to the highly unusual nature of this measurement, a more common high value of 6% that was seen in multiple local anomalies in the first ~2000 sols was used for these models (Jun *et al.*, 2013; Litvak *et al.*, 2014; Mitrofanov *et al.*, 2014).

Input parameter: atmospheric water content

For the purpose of this model, we have assumed a water column abundance of 10 pr µm. Mellon *et al.* (2004) allowed for a water column abundance of 5–30 pr µm, and Mellon typically uses 20 pr µm in ice modeling when considering the recent kyr–Myr history of ice. This is because 20 pr µm offers the best fit to the Mars Odyssey Neutron Spectrometer data (depth of ice and geographic distribution) as per Mellon *et al.* (2004). Note that 5–30 pr µm were not ruled out, but 20 pr µm was the best fit. However, for the M2020 modeling here, we are looking forward from the present not into the past.

At present, what is the water abundance at the surface? The answer will depend on geographic location, elevation, at atmospheric mixing. The last of these is not well constrained. It will also vary substantially with season. There are lots of papers on this topic: 10 pr µm uniformly mixed with CO_2 is a reasonable approximation. However, since ground ice is unstable at any M2020 site, this choice may be academic. Shallow ice would be lost rapidly at the ground temperatures that are relevant to the Mars-2020 landing site, and even faster when ground temperatures are elevated. The rate is proportional to the vapor density gradient between atmosphere and subsurface. If the subsurface vapor density is much greater than the atmosphere's, then a small uncertainty in the atmosphere will not alter the result. Using the Jezero site, for example, 10 pr µm uniformly mixed with CO_2 would have a density gradient of 36 E-9 g/cc, and if the atmosphere had 20 pr µm, the density gradient would be 35 E-9, which is insignificantly different.

Input parameter: mineralogy

To model the mineralogy of the subsurface material, analyses of seven outcrop samples and one sample aeolian material (Rocknest) collected by MSL were considered: CHEMIN analyses of the mineralogy by X-Ray Diffraction were used, and the quantity and timing of volatile release from

SAM measurements during the thermal ramp were also incorporated (Bish *et al.*, 2013; Leshin *et al.*, 2013; Archer *et al.*, 2014).

Input parameter: porosity and permeability

To model the porosity of regolith, undisturbed aeolian sands were used as an analogue. The porosity range given in Kolbuszewski *et al.* (1950) is between 34% and 40%; so for this model, 37% was used. For Mars, this is considered to be at the lower (more restrictive) end of expected values. For disturbed regolith, higher values would be warranted, but we have not modeled that. For permeability measurements, a correlation between average permeability and porosity for sandstone for global petroleum reservoirs shows an average of 2000 mD (with P10 and P90 values of 5000 and 200 mD, respectively) (Ehrenberg and Nadeau, 2005); however, values higher than 30 D have been measured for newly deposited sands. A lower permeability would allow the water to more slowly escape the regolith into the atmosphere, so the 2000 mD value was used for these models to be conservative.

Input parameter: thermal capacity and conductivity

The thermal capacity was calculated by using a single equation for all materials (that was based on lunar basalt) at different temperature ranges (Fujii and Osako, 1973; Sylvain Piqueux, personal communication).

$$\mathrm{Cp}(\mathrm{T}) = (0.0650 + [0.394\mathrm{E}-3] \times \mathrm{T} - [0.452\mathrm{E}3]/\mathrm{T}^2) \times 4184$$

The regolith model assumes a dry soil conductivity of 0.038 W/(m·K). This corresponds to a value that would be frequently derived from global thermal inertia maps as determined from orbit, but it is slightly lower than implied from the measured thermal inertias of the landing sites under consideration by Mars 2020. For example, assuming a density of 1650 kg/m^3 and heat capacity of 850 J/(kg·K), a conductivity of 0.038 yields a thermal inertia of about 230 (MKS units). Actual sites range from 239 to 424 (and the averages for Jezero and NE Syrtis are 297 and 283, respectively). Thus, the figure of 0.038 W/(m·K) is on the lower side of average, but this lower thermal conductivity would be more conservative for heat retention, and in modeling for planetary protection applications, conservatism is commonly practiced. Note that the thermal inertia of Mars surface materials as derived from orbit and on the ground spans about three orders of magnitude, from <40 W · m^{-2}·K^{-1}·s$^{-1/2}$ for the fine dust (~1/4 of Mars) to about >2000 W · m^{-2}·K^{-1}·s$^{-1/2}$ for ices, rocks, or very cemented regolith.

The thermal conductivity of regolith was modeled (Appendix Fig. A1), and is highly dependent on grain size (a sand-equivalent size of 150 µm was used) and hydration (detailed earlier). The model included conductivity variation due to increased evolved water content and rock melting near the heat source (Presley and Christensen, 1997; Wolery *et al.*, 2004); however, this modeling did not take into account the thermal dependence of thermal

conductivity, as it is a minor effect compared with those under consideration here. (In addition, the models do not account for descent of the heat source if the regolith were to actually melt.) Note that the secondary model did not observe temperatures near the source above a regolith melting temperature.

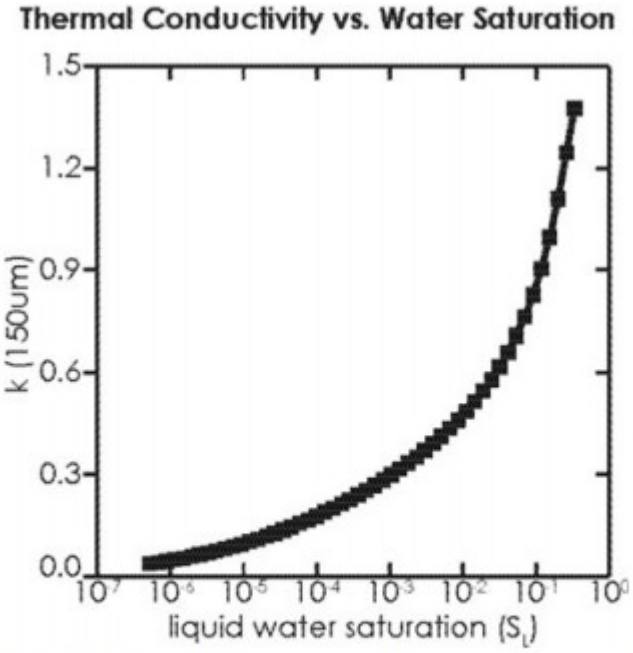

APPENDIX FIG. A1. Assumed thermal conductivity of martian regolith comprised sand-sized (150 µm) grains as a function of liquid water saturation (modeled after Edwards and Piqueux, 2016 and Piqueux and Christensen, 2009a, 2009b).

Input parameter: environmental temperature

In our primary numerical model we needed to choose a single value for the initial temperature. The temperature of the shallow subsurface on Mars is different in different places, so it is obviously not possible to pick a single value that would be valid for the entire planet. In addition, thermal conditions change during the course of the annual seasonal cycle, and the depth scale of the thermal wave is significant relative to the assumed depth of emplacement of the Radioisotope Thermoelectric Generator (RTG). It is not clear what value would plausibly be the most threatening for this parameter, but we thought that a cold end-member might enhance liquid concentration and thermal energy containment. We chose 183 K (the lowest winter temperature for Gale Crater), although these cold winter temperatures only apply to the surface at that location, and would be unrealistically cold at depth. A more generally relevant temperature for the landing sites under consideration by Mars 2020 might be 215–225 K. Note that the regolith at 183 K would be a stable state for ground ice in the current climate (corresponding to 10–20 pr µm) (Mellon and Jakosky, **1993**;

Mellon *et al.*, **2004**). A model run with warmer initial temperatures would have allowed greater peak temperatures, and an acceleration of vapor diffusion, water redistribution, and loss to the atmosphere. The secondary model had the capacity to address the potential effects of variation of the temperature of the surface or atmosphere due to diurnal or seasonal effects.

* The word “saturation” has two different technical meanings, and both are used in this article. It can refer to the thermodynamic state of water, as in the “saturation vapor pressure” (the vapor pressure in equilibrium with the condensed phase), or it can refer to the relationship between solute and solvent (e.g., the words “supersaturation” and “undersaturation”). It can also refer to the volumetric amount of water in the pore space of rock/soil. The latter is the primary usage in this article, and the symbol used to represent it, capital S, is defined in Section 7.1.

References

Archer P.D.Jr., Franz H.B., Sutter B., Arevalo R.D.Jr., Coll P., Eigenbrode J.L., Glavin D.P., Jones J.J., Leshin L.A., Mahaffy P.R., McAdam A.C., McKay C.P., Ming D.W., Morris R.V., Navarro-González R., Niles P.B., Pavlov A., Squyres S.W., Stern J.C., Steele A., and Wray J.J. (2014) Abundances and implications of volatile-bearing species from evolved gas analysis of the Rocknest aeolian deposit, Gale Crater, Mars. J Geophys Res Planets 119:237–254.

Beaty D.W., Buxbaum K., Meyer M., Barlow N., Boynton W., Clark B., Deming J., Doran P.T., Edgett K., Hancock S., Head J., Hecht M., Hipkin V., Kieft T., Mancinelli R., McDonald E., McKay C., Mellon M., Newsom H., Ori G., Paige D., Schuerger A.C., Sogin M., Spry J.A., Steele A., Tanaka K., and Voytek M. (2006) Findings of the Mars special regions science analysis group. Astrobiology 6:677–732.

Bernard D.E. and Farley K.A. (2016) Mars 2020 Rover mission status in 2016 [Reference No. IAC-16-A3.3A.10]. In International Astronautical Conference, Guadalajara, 6 p.

Bish D.L., Blake D.F., Vaniman D.T., Chipera S.J., Morris R.V., Sarrazin P., Ming D.W., Treiman A.H., Downs R.T., Achilles C.N., Morrison S.M., Yen A.S., Bristow T.F., Morookian J.M., Farmer J.D., Crisp J.A., Rampe E.B., Stolper E.M., and Spanovich N.; MSL Science Team. (2013) X-Ray diffraction results from Mars Science Laboratory: mineralogy of Rocknest Aeolian Bedform at Gale Crater. Science 341:1238932.

Boynton W.V., Feldman W.C., Squyres S.W., Prettyman T.H., Brückner J., Evans L.G., Reedy R.C., Starr R., Arnold J.R., Drake D.M., Englert P.A.J., Metzger A.E., Mitrofanov I., Trombka J.I., d'Uston C., Wänke H., Gasnault O., Hamara D.K., Janes D.M., Marcialis R.L., Maurice S., Mikheeva I., Taylor G.J., Tokar R., and Shinohara C. (2002) Distribution of hydrogen in the near surface of Mars: evidence for subsurface ice deposits. Science 297:81–85.

Brass G.W. (1980) Stability of brines on Mars. Icarus 42:20–28.

Carr M.H. (1983) Stability of streams and lakes on Mars. Icarus 56:476–495.

Clifford S.M., Lasue J., Heggy E., Boisson J., McGovern P., and Max M.D. (2010) Depth of the Martian cryosphere: revised estimates and implications for the existence and detection of subpermafrost groundwater. J Geophys Res 115, E07001, doi: 10.1029/2009JE003462.

Cray J.A., Bell A.N., Bhaganna P., Mswaka A.Y., Timson D.J., and Hallsworth J.E. (2013a) The biology of habitat dominance; can microbes behave as weeds? Microb Biotechnol 6:453–592.

Cray J.A., Russell J.T., Timson D.J., Singhal R.S., and Hallsworth J.E. (2013b) A universal measure of chaotropicity and kosmotropicity. Environ Microbiol 15:287–296.

Daubar I.J., Golombek M.P., McEwen A.S., Byrne S., Kreslavsky M., Schmerr N.C., Banks M.E., Lognonné P., Kawamura T., and Karakostas F. (2015) Measurement of the current martian cratering size frequency distribution, predictions for and expected improvements from insight [abstract 2468]. In 46th Lunar and Planetary Science Conference Abstracts, LPI, Houston, TX.

Dickson J.L., Head J.W., and Fassett C.I. (2012) Patterns of accumulation and flow of ice in the mid-latitudes of Mars during the Amazonian. Icarus 219:723–732.

Edwards A.L. (1972) TRUMP: a computer program for transient and steady state temperature distributions in multidimensional systems. National Technical Information Service, National Bureau of Standards, Springfield, VA.

Edwards C.S. and Piqueux S. (2016) The water content of recurring slope lineae on Mars. Geophys Res Lett 43:8912–8919.

Ehlmann B.L. and Edwards C.S. (2014) Mineralogy of the Martian surface. Annu Rev Earth Planet Sci 42:291–315.

Ehrenberg S.N. and Nadeau P.H. (2005) Sandstone vs. carbonate petroleum reservoirs: a global perspective on porosity-depth and porosity-permeability relationships. AAPG Bull 89:435–445.

Feldman W.C., Boynton W.V., Tokar R.L., Prettyman T.H., Gasnault O., Squyres S.W., Elphic R.C., Lawrence D.J., Lawson S.L., Maurice S., McKinney G.W., Moore K.R., and Reedy R.C. (2002) Global distribution of neutrons from Mars: results from Mars Odyssey. Science 297:75–78.

Fujii N. and Osako M. (1973) Thermal diffusivity of lunar rocks under atmospheric and vacuum conditions. Earth Planet Sci Lett 18:65–71.

Golombek M.P., Grant J.A., Kipp D., Vasavada A., Kirk R., Fergason R., Bellutta P., Calef F., Larsen K., Katayama Y., Huertas A., Beyer R., Chen A., Parker T., Pollard B., Lee S., Sun Y., Hoover R., Sladek H., Grotzinger J., Welch R., Noe Dobrea E., Michalski J., and Watkins M. (2012) Selection of the Mars Science Laboratory landing site. Space Sci Rev 170:641–737.

Grant J.A., Golombek M.P., Grotzinger J.P., Wilson S.A., Watkins M.M., Vasavada A.R., Griffes J.L., and Parker T.J. (2010) The science process for selecting the landing site for the 2011 Mars Science Laboratory. Planet Space Sci 59:1114–1127.

Griffin D.M. (1981) Watewater potential as a selective factor in the microbial ecology of soils. In Water Potential Relations in Soil Microbiology, edited by Parr J.F., Gardner W.R., and Elliott L.F., Soil Science Society of America, Madison, WI, pp 141–151.

Haberle R.M., McKay C.P., Schaeffer J., Cabrol N.A., Grin E.A., Zent A.P., and Quinn R. (2001) On the possibility of liquid water on present-day Mars. J Geophys Res Planets 106:23317–23326.

Hammel T.E., Bennett R., Keyser S., Sievers R., Otting W., and Gard L. (2013) Multi-mission radioisotope thermoelectric generator (MMRTG) performance data and application to life modeling [Reference AIAA 2013–3925]. In 11th International Energy Conversion Engineering Conference, American Institute of Aeronautics and Astronautics San Jose, CA, 8 p.

Harris R.F. (1981) The effect of water potential on microbial growth and activity. In Soil Microbiology, edited by Parr J.F., Gardner W.R., and Elliott L.F., Soil Science Society of America, Madison, WI, pp 23–95.

Hecht M.H. (2002) Metastability of liquid water on Mars. Icarus 156:373–386.

Hecht M.H. and Vasavada A.R. (2006) Transient liquid water near an artificial heat source. Mars 2:83–96.

Hecht M.H., Kounaves S.P., Quinn R.C., West S.J., Young S.M.M., Ming D.W., Catling D.C., Clark B.C., Boynton W.V., Hoffman J., and Smith P.H. (2009) Detection of perchlorate and the soluble chemistry of martian soil: findings from the Phoenix Mars Lander. Science 325:64.

Heldmann J.L., Toon O.B., Pollard W.H., Mellon M.T., Pitlick J., McKay C.P., and Andersen D.T. (2005) Formation of Martian gullies by the action of liquid water flowing under current Martian environmental conditions. J Geophys Res Planets 110:E05004.

Ingersoll A.P. (1970) Mars: occurrence of liquid water. Science 168:972–973.

International Association for the Properties of Water and Steam (IAPWS). (2009) Revised release on the equation of state 2006 for H_2O Ice Ih [IAPWS R10-06]. [see also Feistel R., and Wagner W., 2006. A new equation of state for H2O ice Ih. J Phys Chem Ref Data 35:1021–1047; http://www.iapws.org/]

International Association for the Properties of Water and Steam (IAPWS). (2011) Revised release on the pressure along the melting and sublimation curves of ordinary water substance [IAPWS R14-08]. [*see also* Wagner W., Riethmann T., Feistel R., and A. H. Harvey A.H. (2011) New equations for the sublimation pressure and melting pressure of H2O ice Ih. J Phys Chem Ref Data 40: 043103, doi:10.1063/1.3657937; http://www.iapws.org/]

Jun I., Mitrofanov I., Litvak M.L., Sanin A.B., Kim W., Behar A., Boynton W.V., DeFlores L., Fedosov F., Golovin D., Hardgrove C., Harshman K., Kozyrev A.S., Kuzmin R.O., Malakhov A., Mischna M., Moersch J., Mokrousov M., Nikiforov S., Shvetsov V.N., Tate C., Tret'yakov V.I., and Vostrukhin A. (2013) Neutron background environment measured by the Mars Science Laboratory's Dynamic Albedo of Neutrons instrument during the first 100 sols. J Geophys Res Planets 118:2400–2412.

Kolbuszewski J., Nadolski L., and Dydacki Z. (1950) Porosity of wind-deposited sands. Geol Mag 87: 433–435.

Kounaves S.P., Hecht M.H., Kapit J., Gospodinova K., DeFlores L., Quinn R.C., Boynton W.V., Clark B.C., Catling D.C., Hredzak P., Ming D.W., Moore Q., Shusterman J., Stroble S., West S.J., and Young S.M.M. (2010) Wet chemistry experiments on the 2007 Phoenix Mars Scout Lander mission: data analysis and results. J Geophys Res 115:E00E10.

Leshin L.A., Mahaffy P.R., Webster C.R., Cabane M., Coll P., Conrad P.G., Archer P.D.Jr., Atreya S.K., Brunner S.K., Buch A.E., Eigenbrode J.L., Flesch G.J., Franz H.B., Freissinet C., Glavin D.P., McAdam A.C., Miller K.E., Ming D.W., Morris R.V., Navarro-González R., Niles P.B., Owen T., Pepin R.O., Squyres S., Steele A., Stern J.C., Summons R.E., Sumner D.Y., Sutter B., Szopa C., Teinturier S., Trainer M.G., Wray J.J., and Grotzinger J.P.; MSL Science Team. (2013) Volatile, isotope, and organic analysis of martian fines with the Curiosity rover. Science 341:1238937.

Litvak M.L., Mitrofanov I.G., Sanin A.B., Lisov D., Behar A., Boynton W.V., Deflores L., Fedosov F., Golovin D., Hardgrove C., Harshman K., Jun I., Kozyrev A.S., Kuzmin R.O., Malakhov A., Milliken R., Mischna M., Moersch J., Mokrousov M., Nikiforov S., Shvetsov V.N., Stack K., Starr R., Tate C., Tret'yakov V.I., and Vostrukhin A.; the MSL Team. (2014) Local variations of bulk hydrogen and chlorine-equivalent neutron absorption content measured at the contact between the Sheepbed and Gillespie Lake units in Yellowknife Bay, Gale Crater, using the DAN instrument onboard Curiosity. J Geophys Res Planets 119:1259–1275.

Malin M.C. and Edgett K.S. (2000) Evidence for recent groundwater seepage and surface runoff on Mars. Science 288:2330–2335.

Marion G.M., Catling D.C., Zahnle K.J., and Claire M.W. (2010) Modeling aqueous perchlorate chemistries with applications to Mars. Icarus 207:675–685.

McEwen A.S., Ojha L., Dundas C.M., Mattson S.S., Byrne S., Wray J.J., Cull S.C., Murchie S.L., Thomas N., and Gulick V.C. (2011) Seasonal flows on warm Martian slopes. Science 333:740–743.

Mellon M.T. and Jakosky B.M. (1993) Geographic variations in the thermal and diffusive stability of ground ice on Mars. J Geophys Res Planets 98:3345–3364.

Mellon M.T. and Phillips R.J. (2001) Recent gullies on Mars and the source of liquid water. J Geophys Res 106:23165–23180.

Mellon M.T., Jakosky B.M., and Postawko S.E. (1997) The persistence of equatorial ground ice on Mars. J Geophys Res 102:19357–19369.

Mellon M.T., Feldman W.C., and Prettyman T.H. (2004) The presence and stability of ground ice in the southern hemisphere of Mars. Icarus 169:324–340.

Ming D.W., Archer Jr., P.D., Glavin D.P., Eigenbrode J.L., Franz H.B., Sutter B., Brunner A.E., Stern J.C. Freissinet C., McAdam A.C., Mahaffy P.R., Cabane M., Coll P., Campbell J.L., Atreya S.K., Niles P.B., Bell III J.F., Bish D.L., Brinckerhoff W.B., Buch A., Conrad P.G., Des Marais D.J., Ehlmann B.L., Fairén A.G., Farley K., Flesch G.J., Francois P., Gellert R., Grant J.A., Grotzinger J.P., Gupta S., Herkenhoff K.E., Hurowitz J.A., Leshin L.A., Lewis K.W., McLennan S.M., Miller K.E., Moersch J., Morris R.V., Navarro-González R., Pavlov A.A., Perrett G.M., Pradler I., Squyres S.W., Summons R.E., Steele A., Stolper E.M., Sumner D.Y., Szopa C., Teinturier S., Trainer M.G., Treiman A.H.,Vaniman D.T., Vasavada A.R., Webster C.R., Wray J.J., Yingst R.A., and MSL Science Team. (2014) Volatile and organic compositions of sedimentary rocks in Yellowknife Bay, Gale Crater, Mars. Science 343(6169):1245267.

Mitrofanov I., Anfimov D., Kozyrev A., Litvak M., Sanin A., Tret'yakov V., Krylov A., Shvetsov V., Boynton W., Shinohara C., Hamara D., and Saunders R.S. (2002) Maps of subsurface hydrogen from the high energy neutron detector, Mars Odyssey. Science 297:78–81.

Mitrofanov I.G., Litvak M.L., Sanin A.B., Starr R.D., Lisov D.I., Kuzmin R.O., Behar A., Boynton W.V., Hardgrove C., Harshman K., Jun I., Milliken R.E., Mischna M.A., Moersch J.E., and Tate C.G. (2014) Water and chlorine content in the Martian soil along the first 1900 meters of the Curiosity rover traverse as estimated by the DAN instrument. J Geophys Res Planets 119:1579–1596.

Moridis G.J. and Freeman C.M. (2014a) User's manual for the RealGasBrine v1.0 option of TOUGH+ v1.5: a code for the simulation of system behavior gas-bearing geologic media [LBNL-6870E]. Lawrence Berkeley National Laboratory, Berkeley, CA.

Moridis G.J. and Freeman C.M. (2014b) The RealGas and RealGasH_2O options of the TOUGH+ code for the simulation of coupled fluid and heat flow in tight/shale gas systems. Comput Geosci 65:56–71.

Moridis G.J. and Pruess K. (2006) TOUGH+/GasH2O study of the effects of a heat source buried in the Martian permafrost. Proceedings, TOUGH Symposium 2006, Rep. LBNL-60087; Lawrence Berkeley National Laboratory, Berkeley, CA.

Moridis G.J., Kowalsky M.B., and Pruess K. (2008) Tough+Hydrate v1.0 User's Manual: a code for the simulation of system behavior in hydrate-bearing

geologic media. Technical Report LBNL-0149E; Lawrence Berkeley National Laboratory, Berkeley, CA.

Narasimhan T.N. and Witherspoon P.A. (1976) An integrated finite difference method for analyzing fluid flow in porous media. Water Resour Res 12:57–64.

Outer Space Treaty. (1967) Treaty on Principles Governing the Activities of States in the Exploration and Use of Outer Space, Including the Moon and Other Celestial Bodies. Available online at www.state.gov/t/isn/5181.htm

Papendick R.I. and Campbell G.S. (1981) Theory and measurement of water potential. In Water Potential Relationships in Soil Microbiology, edited by Parr J.F., Gardner W.R., and Elliott L.F., Soil Science Society of America Publications, Madison, WI, pp 1–22.

Piqueux S. and Christensen P.R. (2009a) A model of thermal conductivity for planetary soils: 1. Theory for unconsolidated soils. J Geophys Res 114:E09005.

Piqueux S. and Christensen P.R. (2009b) A model of thermal conductivity for planetary soils: 2. Theory for cemented soils. J Geophys Res Planets 114.

Plaut J.J. (2014) A decade of radar sounding at Mars [abstract 1464]. In Eighth International Conference on Mars, July 14–18, 2014; Pasasena, CA, LPI Contrib. No. 1791.

Potts M. (1994) Desiccation tolerance of prokaryotes. Microbiol Rev 58:755–805. Medline,

Presley M.A. and Christensen P.R. (1997) Thermal conductivity measurements of particulate materials: 2. results. J Geophys Res 102:6551–6566.

Reagan M. (2008) Webgaseos online application v1.0. Report LBNL/PUB-3188. Lawrence Berkeley National Laboratory. http://lnx.lbl.gov/gaseos/

Richardson M.I. and Mischna M.A. (2005) Long-term evolution of transient liquid water on Mars. J Geophys Res Planets 110:E03003.

Rummel J.D., Beaty D.W., Jones M.A., Bakermans C., Barlow N.G., Boston P.J., Chevrier V.F., Clark B.C., de Vera J.-P.P., Gough R.V., Hallsworth J.E., Head J.W., Hipkin V.J., Kieft T.L., McEwen A.S., Mellon M.T., Mikucki J.A., Nicholson W.L., Omelon C.R., Peterson R., Roden E.E., Sherwood Lollar B., Tanaka K.L., Viola D., and Wray J.J. (2014) A new analysis of Mars “Special Regions”: findings of the Second MEPAG Special Regions Science Analysis Group (SR-SAG2). Astrobiology 14:887–968.

Sears D.W. and Chittenden J.D. (2005) On laboratory simulation and the temperature dependence of the evaporation rate of brine on Mars. Geophys Res Lett 32:L23203.

Shotwell R., Hays L.E., Beaty D.W., Mellon M.T., Kieft T., Moridis G., and Sypcher N. (2017) Could the impact of the Mars 2020 Power System Into

Martian Regolith Create an Artificial Special Region? [abstract 3630]. In Astrobiology Science Conference (LPI Contrib. No. 1965).

SIERRA Thermal/Fluid Development Team. (2016) SIERRA multimechanics module: Aria user manual-version 4.42 [SAND2016-10166]. Sandia National Laboratories, Albuquerque, NM.

Sizemore H.G. and Mellon M.T. (2008) Laboratory characterization of the structural properties controlling dynamical gas transport in Mars-analog soils. Icarus 197:606–620.

Tokunaga T.K. (2012) Reply to comment by Philippe Baveye on "Physicochemical controls on adsorbed water film thickness in unsaturated geological media." Water Resour Res 48:W11803.

Ulrich R. (2009) Modeling diffusion advection in the mass transfer of water vapor through martian regolith. Icarus 201:127–134.

Wagner W. and Pruss A. (2002) The IAPWS formulation 1995 for the thermodynamic properties of ordinary water substance for general and scientific use. J Phys Chem Ref Data 31:387–535.

Wolery T.J., Jove-Colon C., Rard J., and Wijesinghe A. (2004) Pitzer database development: description of the Pitzer geochemical thermodynamic database data0.ypf. Appendix I in In-Drift Precipitates/Salts Model (P. Mariner) Report ANL-EBS-MD-000045 REV 02. Bechtel SAIC Company, Las Vegas, NV.

Xu J. and Louge M.Y. (2015) Statistical mechanics of unsaturated porous media. Physical Review E. 92. 10.1103/PhysRevE.92.062405.

Zhang G., Spycher N., Sonnenthal E., Steefel C., and Xu T. (2006) Modeling reactive multiphase flow and transport of concentrated solutions using a Pitzer activity approach with TOUGHREACT. J Nucl Technol 164:180–195.